IMPLEMENTABLE CHANGES TO A LARGE-BORE SINGLE CYLINDER NATURAL GAS ENGINE FOR IMPROVED EMISSIONS PERFORMANCE

A Thesis

by

JEFFREY LOUIS BROWN

Submitted to the Office of Graduate and Professional Studies of
Texas A&M University
in partial fulfillment of the requirements for the degree of

MASTER OF SCIENCE

Chair of Committee,	Timothy J. Jacobs.
Committee Members,	Andrea Strzelec
	Jorge L. Alvarado
Head of Department,	Andreas A. Polycarpou

May 2017

Major Subject: Mechanical Engineering

ABSTRACT

In the midst of a controversial time in the energy industry, it is hard to deny the fact that petroleum-based combustion will be a mainstay for many years to come. In light of this reality, it is the task of the engineering community to make natural gas combustion as safe, efficient, and environmentally conscious as possible. This study considers the implementable changes of variable spark timing and reduced cooling fan loads on a natural gas reciprocating-piston internal combustion engine. Emissions are observed over a range of engine speed, engine load, and spark timing conditions.

While active engine controls reduce fuel consumption and emissions, many natural gas pipeline engines in service today operate at set conditions. Each engine can then only be designed to have a small range of optimum performance for a given configuration. While installing controls is possible, it is an expensive endeavor, creating interest in optimizing an engine to its specific operating conditions. This investigation explores emissions and other engine performance data over three engine speeds, three engine loads, and five spark timing configurations on an Ajax E-565 natural gas engine.

In addition to the spark timing study, an investigation into the cooling system is performed to see if and when the engine is exerting wasted energy into cooling itself. The study shows that the engine is in fact supplying too much energy to its fan for moderate climates, warranting further investigation into ways to reduce this parasitic loss.

DEDICATION

To my parents and mentors.

ACKNOWLEDGEMENTS

For as long as I can remember, I have wanted to join the world of engineering, especially working on cars. I am told that I was able to identify vehicles before I had a good understanding of the English language. This interest led me to Texas A&M, and ultimately the Advanced Engines Research Lab.

It is appropriate to begin by acknowledging my cousin, Dean Simpson, for showing me the world of engine research. His enthusiasm for his work while earning his Master's degree made me determined to also pursue this field. His guidance through the process of choosing a University and through the journey of graduate school is largely why I am here today.

One of the best parts of the AERL at Texas A&M University is the camaraderie amongst the researchers. The group is enthusiastic about the work and eager to help each other with whatever challenges arise. My experimental focus on this project gave me the opportunity to work alongside Alireza Mashayekh, who is pioneering a simulation analysis for the engine that I am working on. Not only has his brilliance helped me become a better researcher, but his kindness has made me a better person. I am grateful to have him as a friend along this journey. This project would also not have been possible without the support of Abdullah Bajwa, Tim Kroeger, and Josh Tremblay for working tirelessly to meet our goals.

I am also grateful for the support of my committee members, Prof. Andrea Strzelec and Prof. Jorge Alvarado. Both of these mentors shared their time and

enthusiasm in my work, and have been extremely accommodating in assisting me with my deadlines. I am truly fortunate to be able to have my work reviewed by such talent.

Of course, no study is complete without the guidance of a strong mentor. I am humbled to have had the opportunity to work with Dr. Tim Jacobs, a rare combination of a vastly intelligent engineer and a passionate educator. I remember asking to meet with him as a sophomore, telling him that I was interested in doing engine research. His sincere interest in my endeavors quickly made it clear that I was not only going to have the opportunity to study what I am most interested in, but also do so with a world-class advisor. His positive personality always sees the best in people, and he gives genuine encouragement and inspiration when it seems like everything is falling apart. He is an icon to the internal combustion engine community, and an inspiration to the people around him. Thank you for this opportunity, Dr. Jacobs.

CONTRIBUTORS AND FUNDING SOURCES

Contributors

Part 1, faculty committee recognition

This work was supervised by a thesis committee consisting of Professor Timothy Jacobs [advisor] and Professor Andrea Strzelec of the Department of Mechanical Engineering and Professor Jorge Alvarado of the Department of Engineering Technology and Industrial Distribution.

Part 2, student/collaborator contributions

All work for the thesis was completed independently by the student.

Funding Sources

This work was made possible by GE Oil and Gas.

NOMENCLATURE

AERL	Advanced Engine Research Lab
AFR	Air/Fuel Ratio
Ajax	Ajax E-565; Test Engine
ATDC	After Top Dead Center
BHP	Brake Horsepower
BMEP	Brake Mean Effective Pressure
BTDC	Before Top Dead Center
BTU	British Thermal Unit
CAD	Crank Angle Degree
CFD	Computational Fluid Dynamics
CO	Carbon Monoxide
CO_2	Carbon Dioxide
COV	Coefficient of Variance
DAQ	Data Acquisition System
DI	Direct Injection
EGT	Exhaust Gas Temperature
FID	Flame Ionization Detection
HP	Horsepower
IC	Internal Combustion
IMEP	Indicated Mean Effective Pressure

MEXA	Horiba MEXA-7100D; Emissions Bench
NDIR	Non-Dispersive Infrared Detection
NG	Natural Gas
NI	National Instruments
NOx	Oxides of Nitrogen; NO + NO_2
O_2	Oxygen
ppm	Parts Per Million
ppmC	Parts Per Million, Carbon Atom
RoHR	Rate of Heat Release
THC	Total Hydrocarbons
Φ (Phi)	Equivalence Ratio (<1 is lean, >1 is rich)

TABLE OF CONTENTS

Page

LIST OF FIGURES

Page

LIST OF TABLES

Page

1 INTRODUCTION

1.1 The Natural Gas Infrastructure

The natural gas industry is a cornerstone to the American and worldwide economies, in both its energy value and the infrastructure required to keep it operational. While there are a variety of transportation methods of this fuel, the pipeline is arguably the safest, fastest, and most economical [1]. Conveniently, the engines used to propel the gaseous fuel can be fed by the same gas. The Ajax E-565, the test engine of this investigation, is an example of this. There is strong interest in its performance from both operators in the field as well as government regulation agencies. This challenges engineers with not only maximizing the performance from these engines, but also minimizing fuel consumption and harmful exhaust emissions [2].

Many of the units in service today are antiquated, using technology from the early twentieth century [3]. This leaves many opportunities for improved performance by redesigning major components. However, there is high interest in possible modifications to improve existing units, since replacements are expensive and time-consuming to install. The focus of this study is to propose possible retrofits that can be installed in the field, namely an altered spark pickup bracket (to change spark timing) and a modified cooling fan.

It is important to note that 87% of all U.S. domestic energy production is petroleum based, with a quarter of overall energy from natural gas. This, in conjunction with the 2 million miles of pipeline in the United States alone, gives light to the

immensity of this challenge [4]. Even if minimal, but consistent gains are realized, their impact would be significant if used across the industry.

1.2 Two-Stroke Engine Design

The engines that enable pipeline operation are available in many capacities and variations, from single-site pump jack units to multiple building-sized units forming compressor stations. This scope includes two- and four-stroke derivations, some naturally aspirated and others with forced induction [5]. The focus of this study is the naturally-aspirated two-stroke design. This configuration offers many advantages, especially to the often rugged worksites where these engines operate. The simplicity of a two-stroke engine eliminates the common failure points of traditional four-stroke engines, such as valves, camshafts, and timing sets [6]. The idea of natural aspiration (atmospheric intake pressure, thus lacking a super- or turbocharger) aligns with this minimalistic design. Finally, the modesty of the lubrication system make it more apt to survive frigid environments [7]. These factors are all important to the operator who maintains a fleet of engines, valuing reliability and durability over all else. Oftentimes, engines are installed in desolate and treacherous regions, which makes maintenance dangerous and costly.

While durability is a paramount consideration for these engines, performance is also of high importance. The two-stroke engine design excels in this area as well, benefitting from a power stroke from every down stroke, as opposed to the “skipped stroke” of the four-stroke design. To achieve this, a two-stroke essentially combines the

combustion/expansion stroke and the exhaust stoke into one motion, thus increasing the power density of a given displacement of engine. This is demonstrated in Figure 1-1.

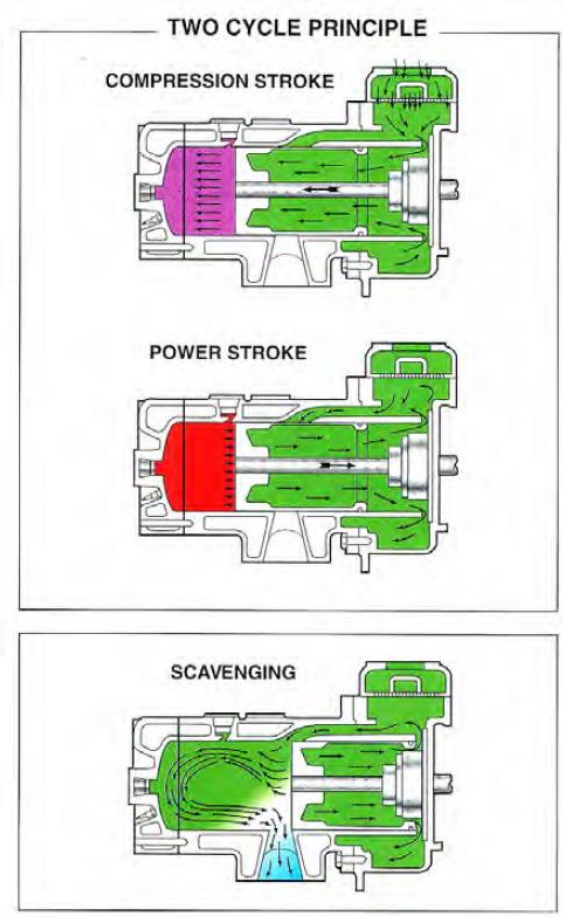

Figure 1-1: The two-stroke combustion process of the Ajax E-565, reprinted from [8]

Another interesting design parameter to consider for two-stroke engines is the in-cylinder turbulence induced by the piston geometry. Because the piston is shaped to expel exhaust gases out of the exhaust ports while simultaneously allowing a fresh mixture in, swirl is induced. This turbulent flow is known to promote a more complete combustion cycle [9, 10]. The geometry of the piston can be seen in Figure 1-2 which is a negative imprint of the piston crown in the engine in this study.

Figure 1-2: Ajax clearance volume mold

1.3 Tradeoffs in an Engine's Operating Parameters

Engine design is a balance between various metrics, nearly always leading to a compromise [11]. It is up to the engine designer and operator to understand the working conditions of their machine, and optimize the engine's characteristics accordingly. For a given engine, its design parameters are best at a specific condition. While parameters are chosen in the design phase, it is only possible to capture the interactions of the variables in an experimental setting.

This idea helped inspire the investigation into the coolant system of the Ajax E-565. This engine is sold as a "one-size-fits-all" unit, which means it must endure the extremes of any environment where it is installed. The engine is known for its durability

in hot climates, so it is likely that the engine is over-cooling itself in moderate conditions, since the engine-driven fan is not actively controlled.

1.4 Effects of Engine Emissions, a Literature Review

An understanding of emissions formation and their effects is necessary in justifying the work done in this investigation. To begin this discussion, a simple stoichiometric combustion reaction between methane and air is given as:

$$\boldsymbol{CH_4 + 2(O_2 + 3.76N_2) \rightarrow CO_2 + 2H_2O + 7.52N_2} \qquad \textbf{1-1}$$

This idealized reaction represents an equivalence ratio of 1, which the engine in this study virtually never realizes [12]. Even when the engine is running at its richest condition, it still does not exceed a phi-value of 0.95. Typically, the engine operates at Φ=0.8. The emissions observed are thus a result of lean combustion. The IC engine community has a strong understanding of how emissions correlate with intake mixture equivalence ratio, which will serve as a validation of the data observed in this investigation [13]. Figure 1-3 depicts the well-documented emissions trends of various exhaust constituents over a range of equivalence ratios.

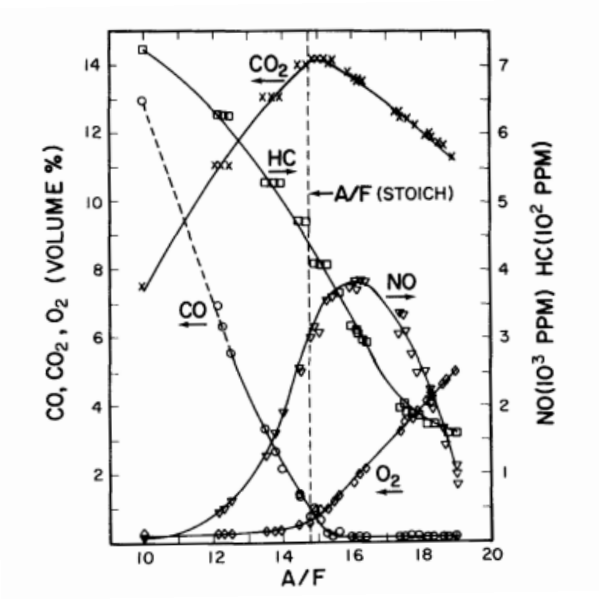

Figure 1-3: Emissions as a function of equivalence ratio, reprinted from [13].

1.4.1 Carbon Monoxide

Carbon Monoxide (CO) is a tasteless, colorless, odorless gas that can cause serious respiratory damage [14]. The fatality rate to those unknowingly exposed exceeds 600 deaths per year, with many other victims suffering from symptoms such as headache, nausea, and fatigue due to hypoxia.

In the context of IC engines, CO is formed from incomplete combustion [15], by not reacting to the final CO_2 state. This is often due to a fuel-rich mixture, where there is not sufficient oxygen to bring the product gas to CO_2. Incomplete combustion can also occur in-cylinder from the engine geometry or operating conditions.

A CO analyzer works on the principle of non-dispersive infrared detection (NDIR) [16]. The exhaust sample flows passed a comparison cell containing N_2, both being exposed to an infrared light. A molecule will absorb infrared energy at a specific

wavelength, and the amount of infrared radiation absorbed by the sample can be measured. This method makes the analyzer useful for a variety of gases.

1.4.2 Unburned Hydrocarbons

A benefit of natural gas combustion over other petroleum combustion is the reduction of CO_2 emissions, a greenhouse gas [17]. However, methane emissions have a similar effect in trapping solar heat when they are in the atmosphere [18]. It is estimated that over the course of a century, methane emissions are nearly 30 times more effective in trapping heat than carbon dioxide emissions [19]. There is strong motivation to reduce these emissions.

Two-stroke engines are notorious for high unburned hydrocarbon (to be referred to as total hydrocarbons, or THC) emissions, due to their tendency to short-circuit fuel directly into the exhaust port [20]. As the intake and exhaust ports are both opened during part of the engine's cycle, the fuel-air mixture from the intake escapes with the exhaust gases. This overlap can be seen in Figure 3-22: Ajax E-565 timing diagram.

The THC analyzer uses what is referred to as FID, or hydrogen flame ionization detection [21]. The analyzer creates a flame with H_2 as a fuel, and introduces exhaust sample gas into this fuel flow. Once the carbon atoms from the sample are exposed to the flame, they emit ions that are detected as current in the machine's electrodes. It is important to note that this method only detects the number of carbon atoms, and cannot distinguish between various hydrocarbons.

1.4.3 Nitrogen Oxides

Nitrogen oxides, commonly referred to as NOx, are comprised of NO and NO_2 [22]. These are highly poisonous gases, and a lead contributor to smog [23]. It is a respiratory irritant when inhaled, and can be fatal. NOx formation is correlated to high temperature, and is formed when nitrogen is oxidized. The following reactions occur between dissociated nitrogen and oxygen (hence, the strong temperature dependence) [24]:

$$N_2 + O \rightarrow NO + N$$
$$N + O_2 \rightarrow NO + O \qquad \textbf{1-2}$$
$$N + OH \rightarrow NO + H$$

Spark timing has a strong effect on NOx formation, as in-cylinder pressures directly correlate to temperatures. Retarding spark timing shifts the peak pressure from combustion past TDC, where the engine sees its highest in-cylinder pressure from the minimized chamber volume. Thus, the net peak pressure is lower, reducing NOx formation. Conversely, advanced timings align peak combustion pressure near the TDC point, resulting in high pressures, temperatures, and NOx formation. This is illustrated in Figure 1-4, showing a clear increase in NOx for the full-advanced timing case [25].

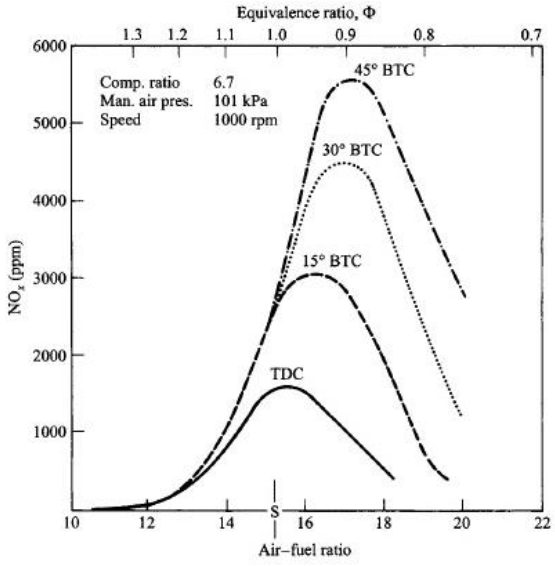

Figure 1-4: NOx concentrations vs equivalence ratio for various spark timings, reprinted from [25]

The analyzer used to quantify NO emissions works on the principle of chemiluminescence [26]. NO is introduce to O_3 in a reactor, resulting in an "excited state" of NO_2, denoted as NO_2^*. This state of NO_2 emits light, which represents how much NO underwent this reaction. The amount of light observed by the analyzer is given as an amount of NO found in the exhaust sample gas. The analyzer observes the following reactions:

$$NO + O_3 \rightarrow NO_2^* + O_2$$
$$NO_2^* \rightarrow NO_2 + light \qquad \textbf{1-3}$$

This method is not capable of measuring the NO_2 from the original exhaust sample, necessitating an additional step for analysis. NO_2 is converted to NO through a reaction with carbon, and can then be analyzed with the other NO constituents in the exhaust sample. This study reports both nitrogen oxides as NOx.

1.4.4 Carbon Dioxide

Carbon dioxide (CO_2) is well-publicized for its ability to trap solar energy in the atmosphere, earning the reputation as being the most significant human-created greenhouse gas [27]. CO_2 analysis is done with the same equipment used to analyze CO, again using the principle of NDIR [16]. The exhaust sample flows past a cell containing N_2, both being exposed to an infrared light. CO_2 is distinguishable from CO because it absorbs a different wavelength of light.

1.4.5 Oxygen

O_2 emissions are helpful in deducing an equivalence ratio when it is difficult to do so at the air and fuel intakes, as is the case with the Ajax engine. Intake air and fuel measurements are not reliable, but oxygen readings prove to be consistent and trend predictably with the engine.

The oxygen analyzer works on the principle of magneto-pneumatic detection [28]. The exhaust sample gas passes through a magnetic field, with its oxygen constituents being attracted to the magnetic poles in the field. The analyzer then measures the increase in pressure at the pole, and corresponds that to an oxygen concentration.

1.4.6 Utilizing In-Cylinder Pressure Data

As discussed, emissions formation are often highly temperature dependent. For the case of an IC engine, the trapped gas will experience an increased temperature when the pressure is increased. There are two main causes for pressure rises in the combustion

chamber – the first is mechanically induced as the piston compresses the mixture, and the second is from the combustion event. The ability to empirically trace both of these curves for various conditions gives insight as to why the emissions are the way that they are.

The pressure data is also used in the derivation of the rate of heat released, expressed in a plot that depicts the energy released from the fuel as a function of crank angle. This is found using Heywood's Gross Heat-Release Rate Equation [29]:

$$\frac{\delta Q_{ch}}{\delta \theta} = \frac{\gamma}{\gamma - 1} p \frac{dV}{d\theta} + \frac{1}{\gamma - 1} V \frac{dP}{d\theta} \qquad \textbf{1-4}$$

The ratio of specific heats for this equation is denoted as γ. A value of 1.3 is appropriate to use for natural gas and thus used for the derivation in this study. The rate of heat release curves give good insight to the effects of spark timing, especially as this directly shifts where the peak pressure due to combustion will occur.

1.5 Objective

The Ajax E-565 engine is a fair representation of other engines in its class, including multi-cylinder and much larger NG engines. While alternative energy technologies are undoubtedly on the rise, the oil and gas industry still has a stronghold on energy cost and capacity. As such, there is great motivation in making antiquated, already implemented technology cleaner. Strategies are being considered in all aspects of the infrastructure, including the well, pipeline, and engines. Considering the

thousands of NG engines used to mobilize gas along the pipeline, a clear understanding of how to make these units cleaner is of interest to operators and government officials alike. The empirical approach of this study aims to improve the exhaust emissions of these legacy engines, both those already in the field and those still to be manufactured in two ways – first, a spark timing sweep over a variety of speed and load conditions. Second, a study of the cooling system is performed to understand if the engine is overloaded in any of the test conditions by its mechanical fan system.

2 EXPERIMENTAL SETUP

2.1 Experimental Procedure for Spark Timing Sweep

2.1.1 Methodology

The parameters that are varied for this study are engine speed, engine load, and spark timing. Engine speed is evaluated in three cases: 350 RPM, 450 RPM, and 525 RPM. The load is set at a percentage of full load, or stalling load, also in three cases: 50%, 75%, and 100%. Finally, spark timing is observed at 1.2, 6.2, 11.2, 16.2, and 21.2 CAD BTDC. The timing that the engine is sold with is 11.2 CAD BTDC; the test sweep includes a range 10 CAD advanced and 10 CAD retarded of the conventional location. The device used to sweep the spark timing can be seen in Figure 2-1: Mechanical spark timing controller.

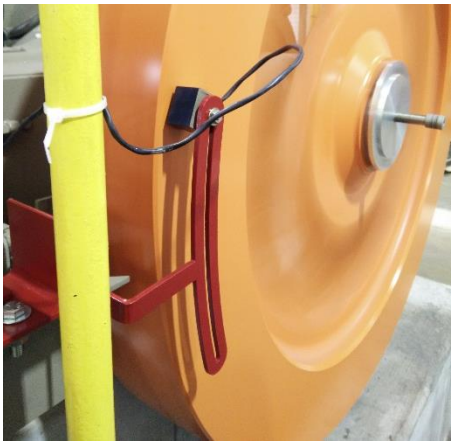

Figure 2-1: Mechanical spark timing controller

To analyze each combination of these variables, 45 distinct test conditions are observed, as shown in Table 1. Each configuration is observed twice, in a random order, ensuring repeatability and reducing the effect of hysteresis. It is important to note that

one test condition – 350 RPM, 100% load, and 10 CAD retarded timing was unsustainable; the engine simply could not maintain this condition. Because of this, 44 test conditions are presented. To accurately acquire emissions data, the engine must reach a steady-state condition. This is verified by observing the exhaust temperature. Once the EGT stabilizes, the emissions readings are taken, and the DAQ observes 300 sequential cycles to write a summary file of the in-cylinder pressure data. Throughout the test cases, the engine stabilized between 8 and 12 minutes.

Test Condition	Engine Speed (RPM)	Engine Load (%)	Spark Timing (CAD BTDC)
1	350	50	1.2
2	350	75	1.2
3	350	100	1.2
4	350	50	6.2
5	350	75	6.2
6	350	100	6.2
7	350	50	11.2
8	350	75	11.2
9	350	100	11.2
10	350	50	16.2
11	350	75	16.2
12	350	100	16.2
13	350	50	21.2
14	350	75	21.2
15	350	100	21.2
…	…	…	…
45	525	100	21.2

Table 1: Data matrix for three test parameters

2.1.2 Data Analysis

Engine exhaust emissions are something that have been studied for many decades, both for their polluting and greenhouse gas effects [23, 30, 31]. This study quantifies the NOx, CO, CO_2, THC, and O_2 that is emitted from the exhaust during each

test condition. NOx and CO have especially harmful respiratory affects that are required to be minimized [22]. The interactions between each constituent is fascinating, and previous studies suggest strong correlations between them [32]. These known trends help explain the results seen from the study.

In-cylinder pressure reveals much about what is occurring inside the combustion chamber, as it can be used to derive the rate of heat released by the mixture [29]. This pressure data is useful to the engine experimentalist, as the data is time-variant (rather, compared to piston position), thus allowing for the start and propagation of combustion to be visualized [33]. This data, in addition to a chemical understanding of exhaust emission formation mechanisms, allows researchers to more accurately reduce emissions. In fact, correlations between pressure data and NOx emissions have been found in literature to be strong enough to be able to program an engine controller [34].

2.2 Experimental Procedure for Coolant System Study

2.2.1 Methodology

The second part of this study is an investigation into the load that the cooling system imposes on the engine, and if any action could be taken to reduce this [35]. The thermo-siphon cooling system on the Ajax test engine has no pumping mechanism; its flow is induced by the density gradient between region around the combustion chamber and the radiator [6]. The radiator is cooled by natural convection, as well as a belt-driven fan from the crankshaft. However, the fan has no controls – when the engine spins, so

does the fan, and at a proportional rate. The system is illustrated in Figure 2-2, with the thermal gradients and fluid flow direction shown.

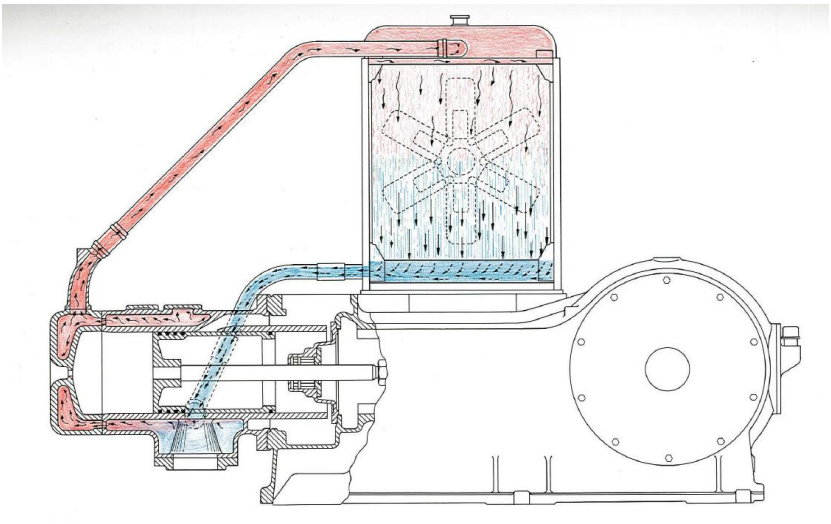

Figure 2-2: Principle of thermo-siphon cooling, reprinted from [6]

A system like this is optimized for one working condition (likely, the harshest), and can cause a significant, unwarranted load in other conditions. This design recalls the aforementioned discussion on reliability and durability, yet opens a door for efficiency improvements. A study into how this cooling system can be improved is included in this overall investigation.

Since the flow inside the cooling jacket has no pump, any instrumentation used to assess the flowrate cannot be too restrictive, as this could starve the engine of coolant and overheat it. A venturi-style flowmeter is commercially available for the coolant pipe size on the engine, and doesn't over-restrict the system. A manometer is fitted to the flowmeter to observe the pressure drop across the venturi, a value necessary for the flowrate derivation. The system designed to measure the coolant flowrate specifically for this engine is outlined in Figure 2-3: Flowmeter installed on cooling system.

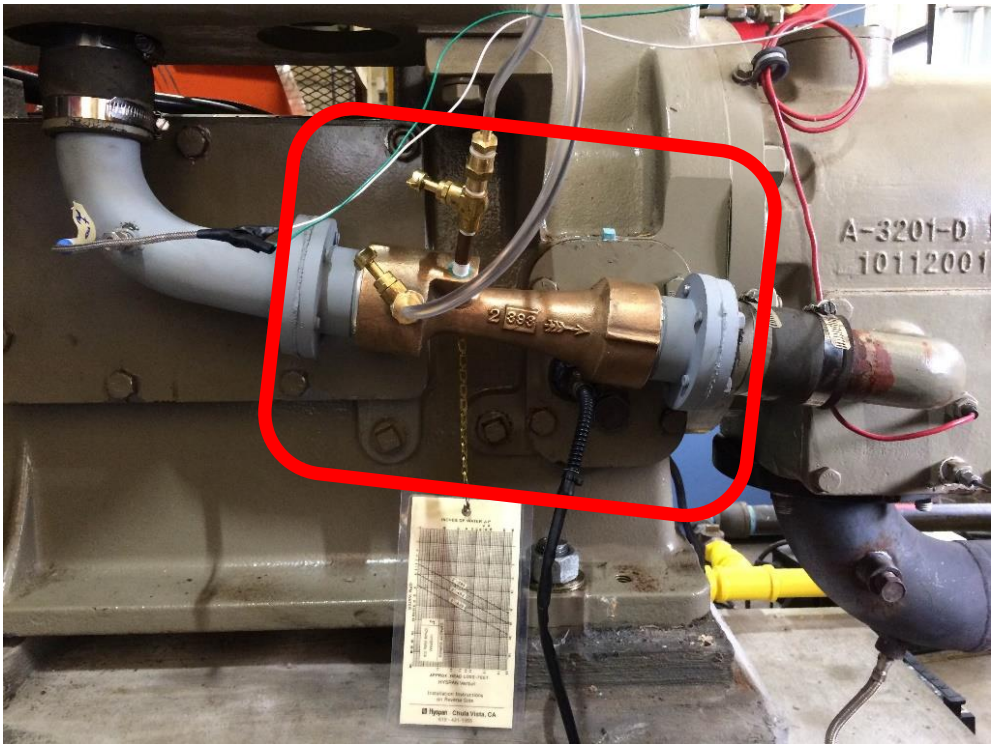

Figure 2-3: Flowmeter installed on cooling system

The coolant pipes are instrumented with thermocouples in four locations – before and after the water passes over the combustion chamber, and before and after the water falls through the radiator. T-type thermocouples are used for their accuracy in the expected temperature range [36]. This data is used for the derivation of flowrate, as the density of the working fluid is necessary for the calculation. It is also used to calculate how much heat is added to the system from the combustion events and how much is removed from the radiator. Figure 2-4 depicts the thermocouple location on the upper coolant pipe before the radiator.

Figure 2-4: Thermocouple mounted before radiator

2.2.2 Data Analysis

The metric for determining "effectivity" of the cooling system on the Ajax E-565 is the heat transfer rate across the radiator. In order to complete this calculation, the flowrate of the coolant must be quantified. Information from the flowmeter and the coolant temperature derive flowrate, based on the continuity equation. The flowmeter is fit with a manometer across the venturi. Once the engine reaches steady state, the readings are taken across both lines, resulting in a pressure differential. The ratio of inlet to throat diameter, denoted as the beta ratio, is given by the manufacturer to be 393.

The expansion coefficient (Y) is 1, since the working fluid is water. The temperature used to find the density of the coolant is found from the thermocouple downstream of the radiator. The observed temperature is immediately before the inlet of

the venturi, giving the high accuracy to the state of the coolant where it is measured. These calculations are shown in Appendix C - Coolant Flowrate.

The heat transfer rate across the radiator is derived from the heat equation, using the flowrate derived in the aforementioned calculations. This equation can be found in Appendix C - Heat Transfer Rate. The temperatures used for this derivation are helpful in seeing how much heat is input into the cooling system by the combustion chamber and how much is removed by the radiator. The engine can be determined to be removing too much heat if the water temperature does not reach or exceed its boiling temperature. In addition to quantifying heat removal and determining if it is an appropriate, it is useful to the AERL team to know how different speeds and loads affect heat input into the cooling system, a sign of wasted energy.

2.3 Equipment

2.3.1 Engine

The engine of interest for this study is the Ajax E-565, as show in Figure 2-5. This is a 9.3L displacement, two-stroke, single-cylinder, naturally aspirated engine. The bore measures 8.5” and the stroke 10” [8]. It is damped by a 48” diameter, 1,500 lbs. flywheel. Further details on the engine can be found in Table 2: Ajax E-565 specifications.

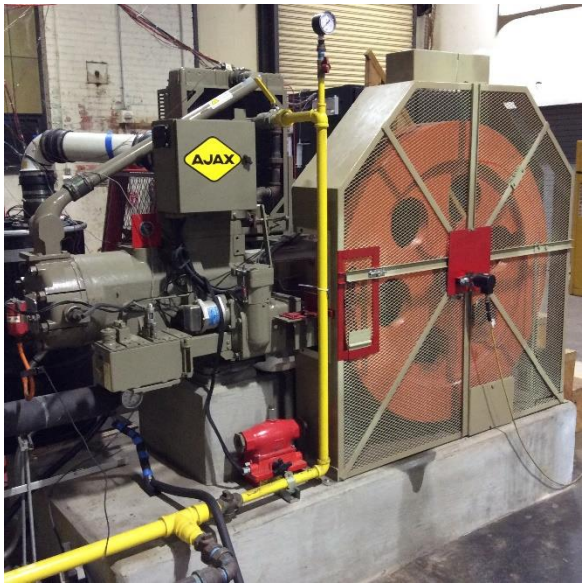

Figure 2-5: Ajax E-565 at Texas A&M AERL

The gas composition that is burned in the engine is sourced from the city of College Station, TX and is roughly 93% methane, 4% ethane, and the remainder heavier hydrocarbons, nitrogen, and carbon dioxide. A detailed composition report is found in Appendix A. The gas is manually controlled by a mechanical valve that feeds the stuffing box prior to being inducted into the combustion chamber.

Rated Continuous BHP at 100° F (38° C) Ambient	40 HP (29.8 kW)
Rated RPM	525
Bore x Stroke	8-1/2" x 10" (216 mm x 254 mm)
Piston Displacement	567 in^3 (9.29L)
Rated Piston Speed	875 ft/mn (267 m/min)
Weight (including flywheel)	4716 lb (2139 kg)
BMEP	53.6 psi (3.67 kg/cm^2)
Compression Ratio	6:01
Torque	400 ft-lb (542 N-m)

Table 2: Ajax E-565 specifications

The engine is instrumented with both air and fuel measuring equipment, however neither are able to provide useful data. This is attributed to the oscillatory intake-purge process that occurs in the stuffing box and the fact that there are not multiple cylinders with shifted intake phasing to smooth out this pressure data. In an attempt to mitigate these effects, a surge tank is installed in the gas line (Figure 2-6), which acts as a gas intake plenum to reduce the observed pulsations [37].

Figure 2-6: Surge tank installed in gas line

Gas flow readings are still unusable with this installation. Fuel flow rate data is helpful to determine fuel consumption and equivalence ratio, which must be hypothesized from emissions data after combustion.

2.3.2 Dynamometer

The engine resides in an enclosed laboratory setting, and has a mechanical clutch connecting to a Taylor eddy-current dynamometer. The 150 HP, 3,500 RPM full load capabilities of this dyno far exceed what the Ajax is capable of producing [38]. The load is manually controlled with a potentiometer, setting voltages with a Fluke voltmeter to calibrated torque loads. The physical specifications are found in Table 3: Taylor dynamometer specifications, DEA150. The engine/dyno setup are seen in Figure 2-7: Taylor dynamometer.

Length	17.5 in	444.5 mm
Mounted Holes - Width	39.13 in	993.9 mm
Height	49 in	1,245 mm
Weight	1300 lbs.	590 kg
Heat Load from Dyno (per hour)	115 kW	382,000 BTU

Table 3: Taylor dynamometer specifications, DEA150

Figure 2-7: Taylor dynamometer

2.3.3 Data Acquisition System

The DAQ system is largely comprised of components by National Instruments. The NI system has input signals from an encoder (engine speed), pressure transducer (in-cylinder and otherwise), and various temperature measurements. The real-time ability of this system allows for a range of engine parameters and their interactions to be observed. Pressure curves are calibrated by phasing BDC to the atmospheric pressure of the area during the testing. This condition is analyzed at ambient pressure, since the exhaust port is equalized with the atmosphere. The user interface is shown in Figure 2-8.

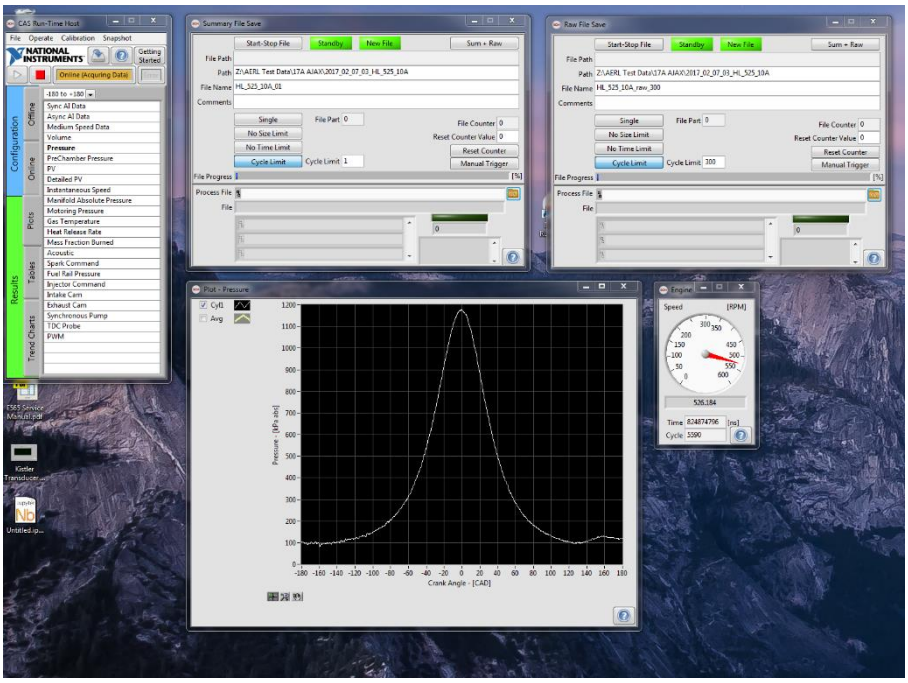

Figure 2-8: User interface for DAQ

The primary information gathered from the DAQ is in-cylinder pressure as a function of crank angle. After the engine reaches steady state for a condition, a summary file of 300 consecutive cycles is compiled to give an average pressure curve. This is useful in not only comparing peak pressures between conditions, but also seeing where in the cycle they occur. If, for example, the peak pressure is too far advanced, some of the heat released is during the compression stroke, thus expanding against the direction of piston motion. The pressure curve is also utilized in deriving the rate of heat released curve, which evaluates engine performance as well as explains exhaust emissions trends.

2.3.4 Emissions Monitoring Equipment

Engine exhaust emissions, specifically NOx, THC, CO, CO_2, and O_2, are recorded and analyzed for this study. This is done with the Horiba MEXA-7100D

emissions bench. The user interface for the equipment is shown in Figure 2-9. Before each use, the analyzers are purged with nitrogen for roughly 10 minutes to remove any condensation that may contaminate the data. Also, before each test campaign, the analyzers are zeroed and calibrated to a span gas of known concentration.

Figure 2-9: MEXA-7100D user interface

3 RESULTS AND DISCUSSION

3.1 Emissions

Exhaust emissions and in-cylinder pressure data are acquired after the engine is shown to have reached steady-state conditions, confirmed by a stabilized exhaust gas temperature. Of the 45 test conditions in the test matrix, one was not able to be sustained: at 350 RPM, fully retarded spark timing, and full load. As such, the following data points are from 44 test conditions, each being run twice. The test condition order was randomized between the two test campaigns to minimize any effects of previous conditions, or hysteresis.

While consistent and expected trends are apparent with the results, some conditions present a lot of uncertainty. This is an expected reality, given the type of engine in this study. The slow-speed, single-cylinder, large-bore design induces significant cyclic variation. The slow speed of the engine prolongs the interaction between the intake and exhaust ports, allowing this fresh charge to affect exhaust emission constituents in an inconsistent manner. This, of course, is also consequence of the two-stroke design. The single-cylinder design complicates readings because the piston oscillations are not balanced as they would be in a multi-cylinder engine. This is the same reason that intake air and fuel readings cannot be taken with certainty. Finally, the large-bore chamber adds uncertainty to the mixture interactions (such as turbulence, swirl, etc.) and mixture homogeneity, which is a significant parameter in an emissions analysis.

Another consequence of this is an inability to accurately measure air and fuel intake rates to the stuffing box. Even though both channels have large surge tanks to suppress the pressure oscillation, flowmeters on these channels cannot give consistent reading. An important observation regarding equivalence ratio effects for various test cases – while there is no direct measurement of how much fuel is fed to the engine, it was consistently apparent that the retarded spark timing cases required significantly more fuel to keep the engine from stalling, making those cases notably richer than the standard and advanced timing cases. Equivalence ratio will be further discussed based on emissions trends.

3.1.1 Engine Stability

While the nuances of the two-stroke, large bore engine inherently lead to high uncertainty in some measurements, it is possible to relatively quantify how stable each engine configuration is. The term used for this is the COV of IMEP, or the coefficient of variance of the indicated mean effective pressure [39]. IMEP is a normalized parameter dividing work produced per cycle by the displaced volume per cycle [40].This is ratio of the standard deviation of the in-cylinder pressure divided by the mean of this data, as found over 300 cycles. This ratio represents the variation of work output of the engine; higher values indicated lower combustion stability

The trends of COV of IMEP support what is qualitatively observed during testing – most significantly, that increasing the engine load reduces misfires. The most extreme cases of cyclic variation are at 50% load, with the low speed, fully advanced case nearing a COV ratio of 1. At full load, all engine speeds and ignition timings have a

COV of IMEP below 10%. These trends are shown in Figure 3-1, Figure 3-2, and Figure 3-3.

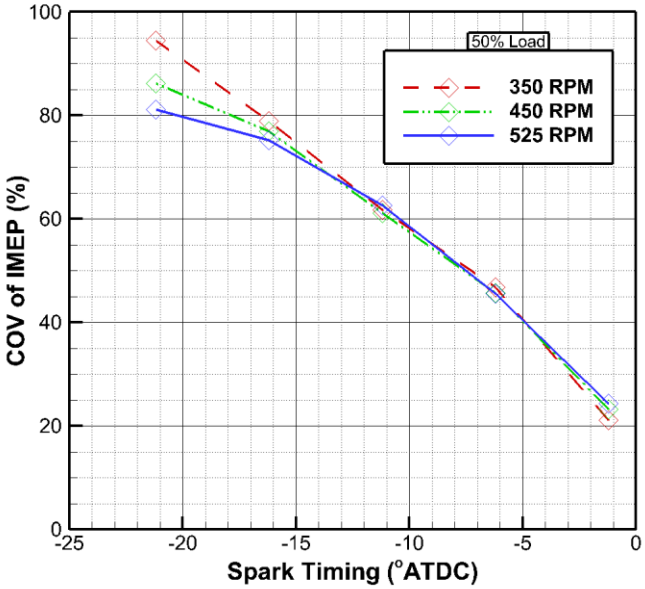

Figure 3-1: COV of IMEP at 50% Load

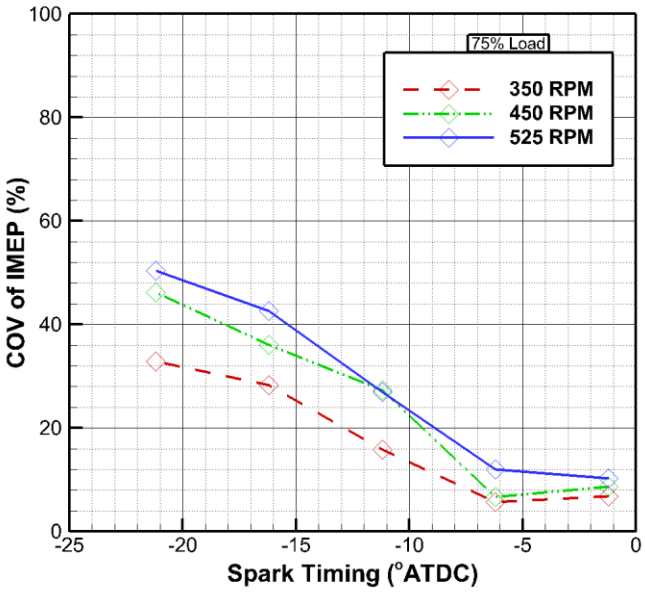

Figure 3-2: COV of IMEP at 75% Load

These illustrations are used in the discussion of the emissions trends seen in the following sections. Specifically, the NOx emissions at high load are much higher than low loads. This correlates to the high combustion stability at high load, increasing the in-cylinder temperature. The misfires observed at low load cases not only add less heat from combustion to the cylinder, but also convectively cool the cylinder walls as the fresh mixture cycles through.

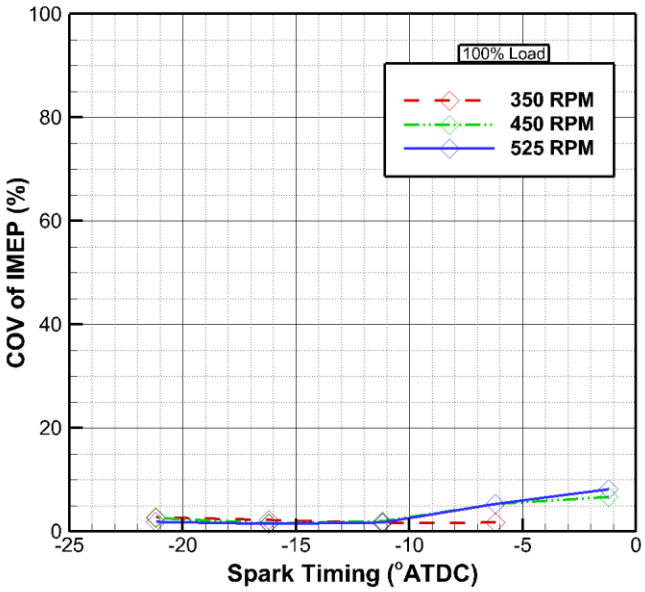

Figure 3-3: COV of IMEP at 100% Load

3.1.2 Carbon Monoxide

CO is traditionally prevalent in fuel-rich mixtures, as there is not enough O_2 to oxidize the carbon atoms to CO_2. The trends from the low-load case appear to follow this theory – as spark timing is retarded, more fuel is required to keep the engine from stalling. However, the trend is not shown with enough statistical significance to say with certainty, as seen in Figure 3-4, Figure 3-5, and Figure 3-6. Due to the lean-running nature of the engine in all conditions, the relatively low CO values never increase significantly.

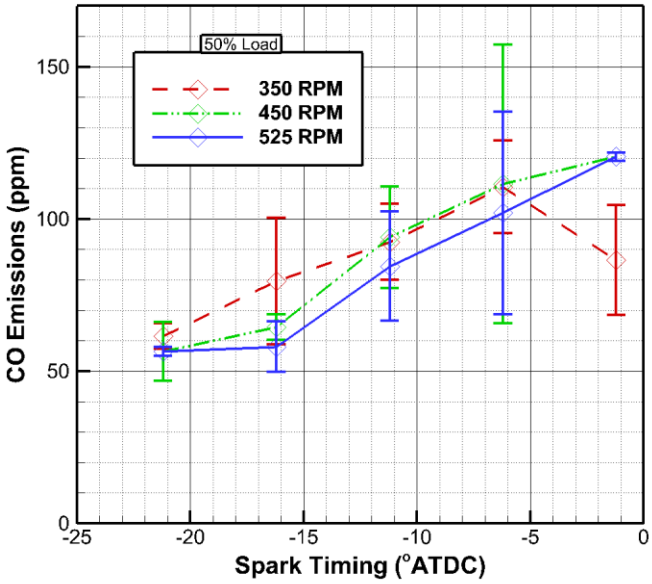

Figure 3-4: CO emissions at 50% load

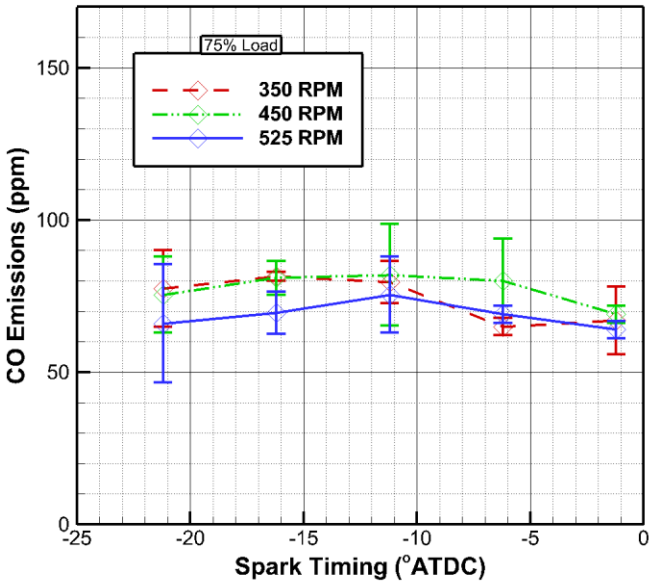

Figure 3-5: CO emissions at 75% load

A stronger explanation for the observed behavior is that there is not enough combustion energy at low load to complete the reaction to CO_2, "freezing" the constituents in their CO state. The flame is not able to completely propagate through the large cylinder cavity.

The range of CO emissions for the 75% and 100% load cases are similar, again with the 95% confidence intervals for many of the data points overlapping. However, the general trend is for an increased engine load to reduce CO emissions, suggesting more complete combustion at high-load cases. This lack of drastic trends between speed, load, and spark timing suggests incomplete combustion for most of the Ajax engine's operating conditions.

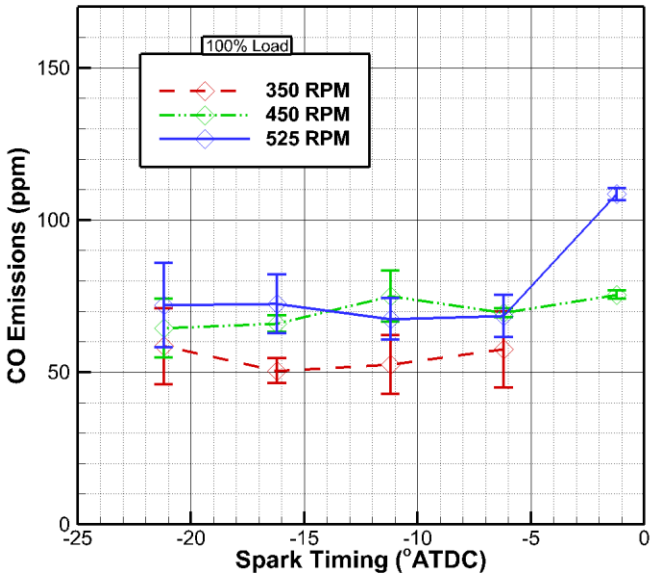

Figure 3-6: CO emissions at 100% load

3.1.3 Unburned Hydrocarbons

THC emissions production for two-stroke engines is largely contributed to the short-circuiting phenomenon, where the intake fuel is directly exhausted [41]. There are approximately 80 CAD where the intake and exhaust ports are interacting with the combustion chamber simultaneously, as illustrated in Figure 3-22: Ajax E-565 timing diagram. With this in mind, the observation that slower engine speeds contribute to higher unburned hydrocarbons is expected, as each CAD takes more time to complete, giving the fuel more time to short-circuit. Cases where more fuel is introduced to the mixture will contribute to THC emissions, corresponding with reduced O_2 emissions. These expected trends are more apparent in the O_2 results than the THC data.

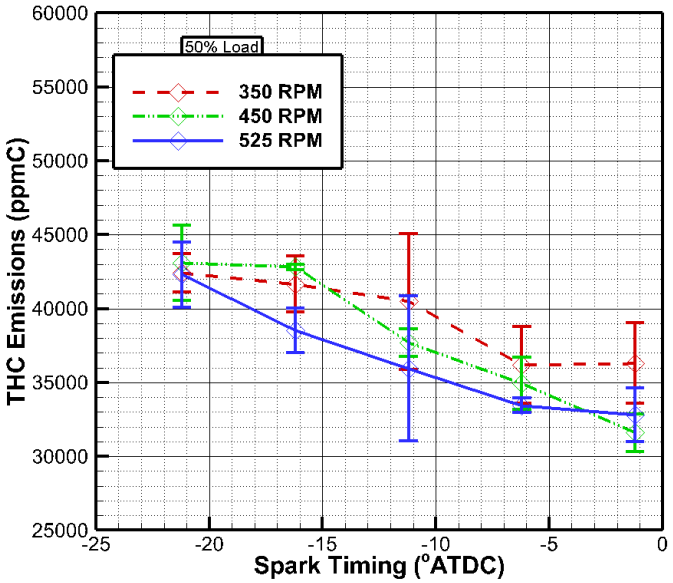

Figure 3-7: THC emissions at 50% load

Engine load trends inversely with THC emissions, although not drastically. The engine's stability is stronger at high load, reducing misfire events. This reduces THC in

the sample, since a misfire results in raw fuel being directly exhausted. This is apparent in the trends of CO_2, which also increase with load, a sign of complete combustion. The outlier in this discussion is the high load, low speed case, having consistently higher values than the other speeds. There are two variables that can explain this. In order to maintain low speed at the high load, significantly more fuel was introduced into the mixture. Again, this is the only configuration that resulted in an unsustainable test case. Also, the slow speed means that the overlap of the intake and exhaust port openings allows more fuel to escape combustion. Outside of the low speed, high load case, there is too much uncertainty to definitively explain the trend of THC emissions with speed, as seen in Figure 3-7, Figure 3-8, and Figure 3-9.

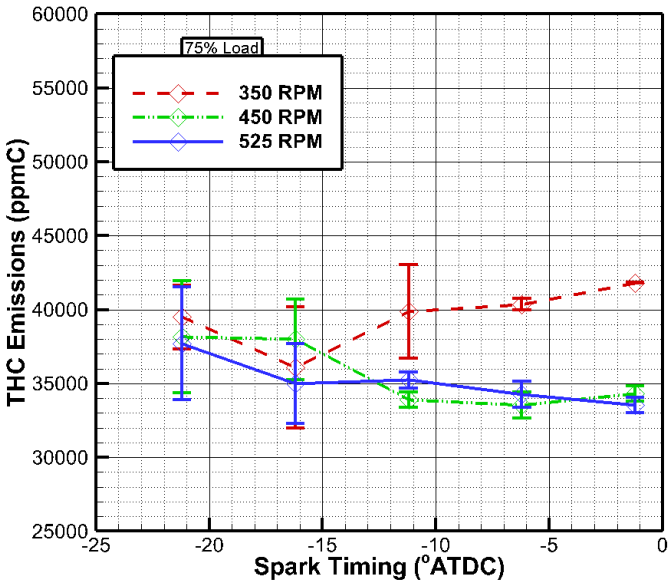

Figure 3-8: THC emissions at 75% load

Retarding spark timing is expected to increase THC emissions, because a richer mixture is needed to sustain the same load and the combustion is less complete. However, this trend is not seen in the data. The low load case even suggests that retarding timing reduces THC emissions. The low load cases have the most misfired events, which may be due to an advanced spark not successfully igniting the mixture. As with speed, the confidence intervals overlap in such a way that a strong conclusion cannot be justified.

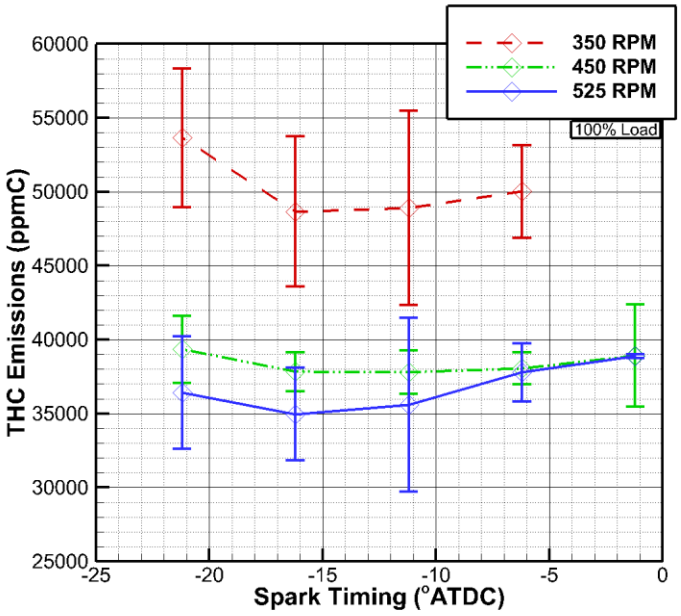

Figure 3-9: THC emissions at 100% load

3.1.4 Nitrogen Oxides

NOx emissions data are the only values from this study requiring a magnified scale to be able to compare all three load cases against each other, as the range is so large. Other studies that compare NOx with spark timing see similarly large ranges,

relieving concern that the values are erroneous [3, 42]. This shows that increasing the load increases NOx formation drastically – high load cases can reach nearly 2000ppm, while low load cases read so low as to suggest reaching the analyzer's minimum detection limit [43]. There is good reasoning to justify this. First of all, as load is increased, the COV of IMEP decreases [3]. This means that the engine has higher stability, and is misfiring less. The result of stable combustion is an increase in temperature, a known strong contributor to NOx formation. At low load, the engine misfires frequently, reducing temperature by both convectively cooling the combustion chamber as well as reducing the heat produced from a successful firing event. Additionally, for the engine to be able to sustain the high loads, the equivalence ratio must be increased. The Φ-values required for high loads approach that of peak in-cylinder temperature, again adding to the thermal NOx mechanism.

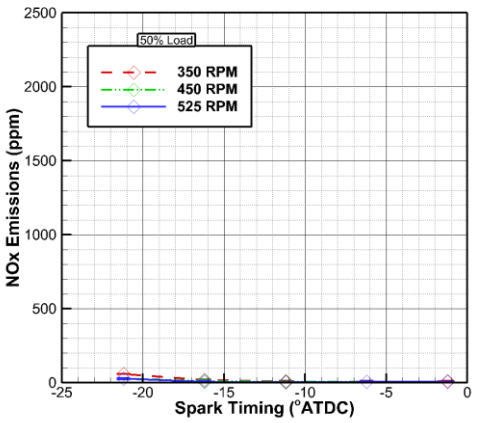

Figure 3-10: NOx emissions at 50% load

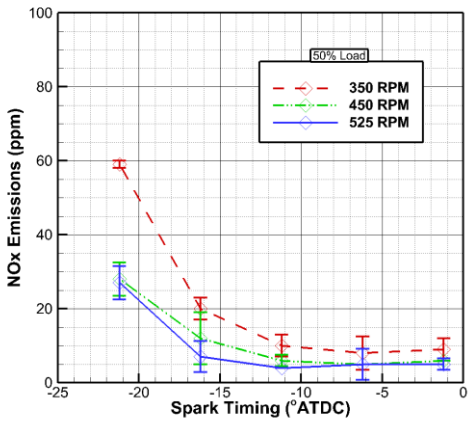

Figure 3-11: NOx emissions at 50% load, magnified

The effects of engine speed are not as clear to deduce, due to the high uncertainty of the measurements. The trend from all load conditions suggests that increasing the

speed reduces NOx formation, a result that may be explained by the cooling system. The cooling fan is mechanically connected to the engine's crankshaft, and rotates proportionally. At high speeds, the fan is removing much more heat from the cooling system, which may be reducing in-cylinder temperatures. The radiator inlet temperature is similar between high and low speeds when fully loaded, yet the heat removed is substantially more for the high speed case, as seen in Table 5.

This data suggests that the engine is more efficient with heat removal at high speeds than at low speeds, which can be seen in Figure 3-10, Figure 3-12, and Figure 3-14. With this hypothesis in mind, it would be of interest to instrument the combustion chamber with a thermocouple in the future to directly measure in-cylinder temperatures for various cases.

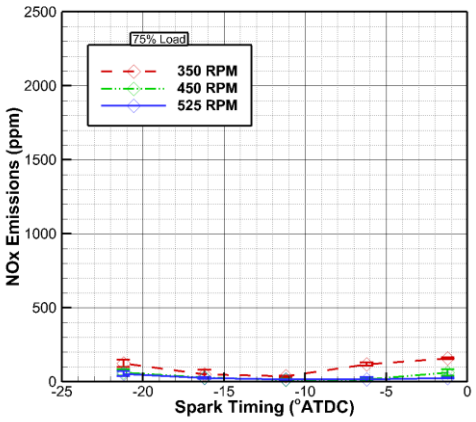

Figure 3-12: NOx emissions at 75% load

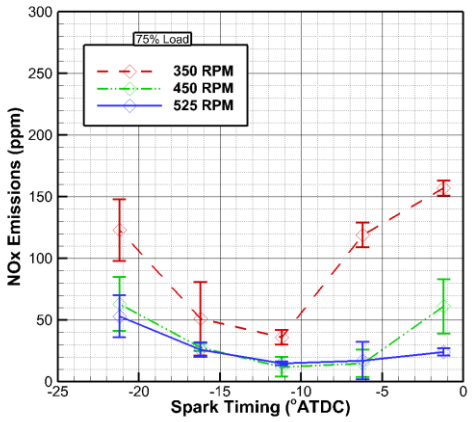

Figure 3-13: NOx emissions at 75% load, magnified

Unfortunately, as with engine speed, the uncertainty between the various timing cases makes a definitive conclusion difficult. However, the apparent trends confirm what is found in literature and confirms what should be happening in-cylinder. As spark

timing is retarded, the combustion pressure curve shifts passed TDC, or the minimum chamber volume condition. This results in a lower overall pressure and temperature, reducing N_2 dissociation and NOx formation. These trends are verified by the pressure data found for the rate of heat release data given in a following section.

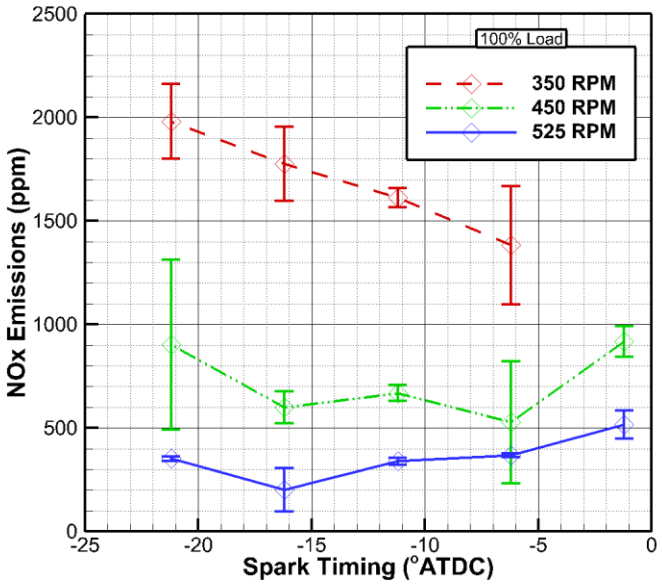

Figure 3-14: NOx emissions at 100% load

3.1.5 Carbon Dioxide

Recalling Equation 1-1, CO_2 emissions are the result of a complete combustion reaction. An expected trend is to see CO_2 and CO emissions inversely related. The CO_2 results appear to compliment the CO results, while also showing trends with respect to spark timing, something not seen in the CO data. As load is increased, so are CO_2 emissions values, likely due to a more thorough combustion process.

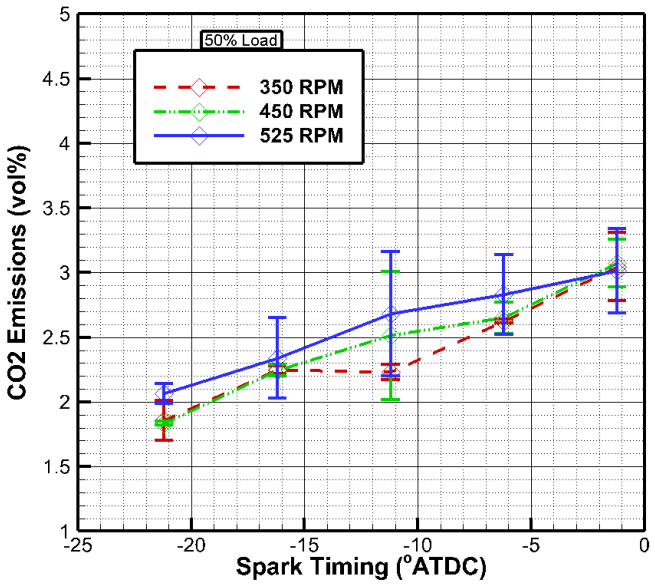

Figure 3-15: CO_2 emissions at 50% load

The impact of engine speed cannot be stated with any confidence due to overlapping error margins, except for the 350 RPM, 100% load condition. CO_2 emissions do clearly directly correlate with load, an expected outcome. As load is increased with this engine, so is the firing stability, resulting in better burning.

CO_2 increases with retarded timing as the mixture is richened. Recall that a richer mixture is still lean of stoichiometric for this engine, meaning that a richer case brings the flame temperature closer to its peak. The peak flame temperature for a flame occurs just rich of an equivalence ratio of 1. The trends seen in Figure 3-15, Figure 3-16, and Figure 3-17 are justified by what is found in literature.

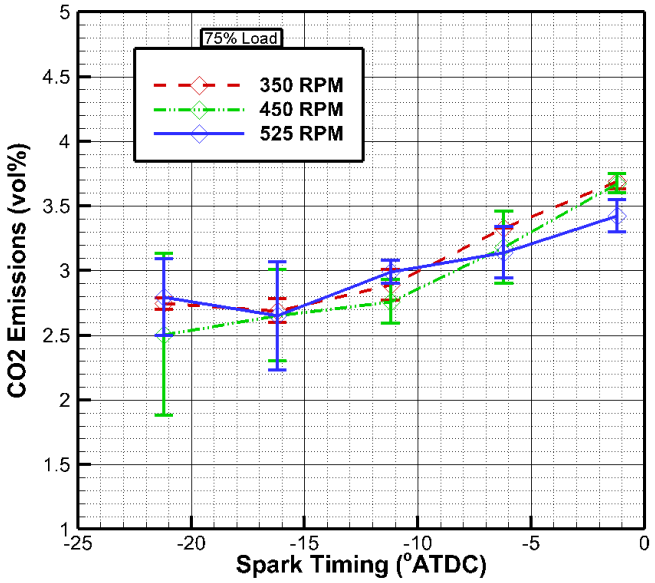

Figure 3-16: CO_2 emissions at 75% load

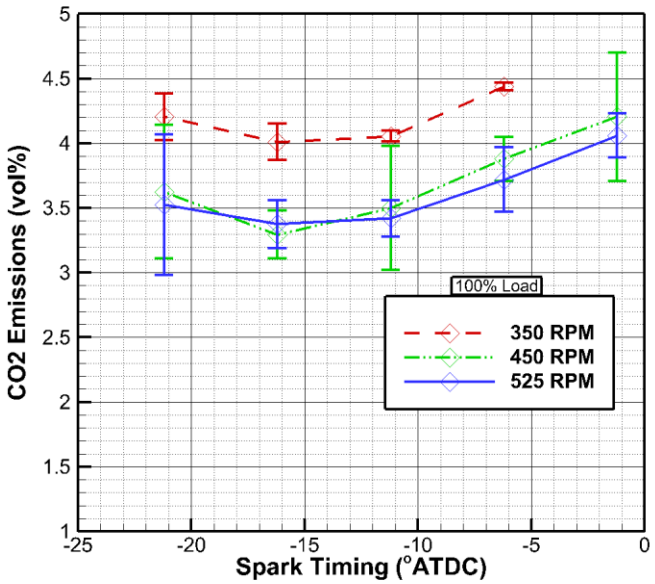

Figure 3-17: CO_2 emissions at 100% load

3.1.6 Oxygen

O_2 constituents in the exhaust are a good indication of how lean a mixture is [44]. Given the poor fuel and air measuring capabilities of this engine test cell, these emissions offer some of the best indication to the equivalence ratio for each test condition. Fortunately, the O_2 readings exhibit predicable behavior, lending validation to the emissions results as a whole. Retarding spark timing removes oxygen content from the exhaust, implying an increased equivalence ratio as spark timing is delayed. Throttle requirements to maintain load during testing confirm this.

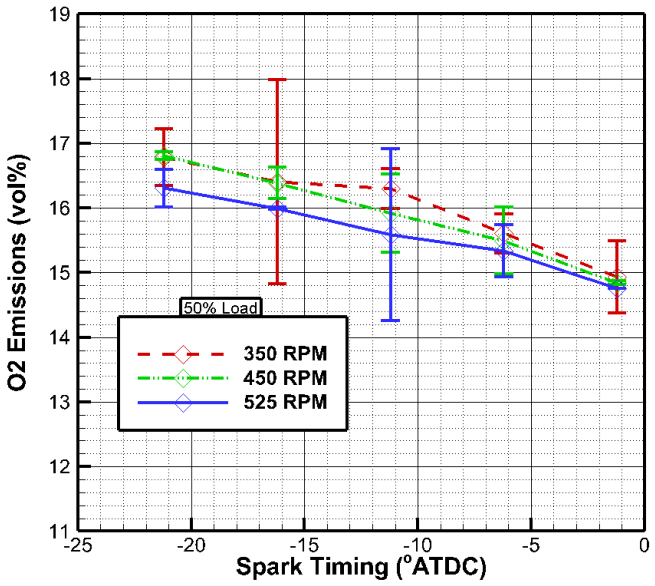

Figure 3-18: O_2 emissions at 50% load

Increasing the load results in a decrease of oxygen in the exhaust samples. In order to maintain the high load cases, the gas throttle is noticeably opened to allow for more fuel to enter the combustion chamber. This increases the equivalence ratio (adding

more fuel) to maintain the higher load. This pattern serves as another validation for the data collected – a higher work demand warrants higher energy input.

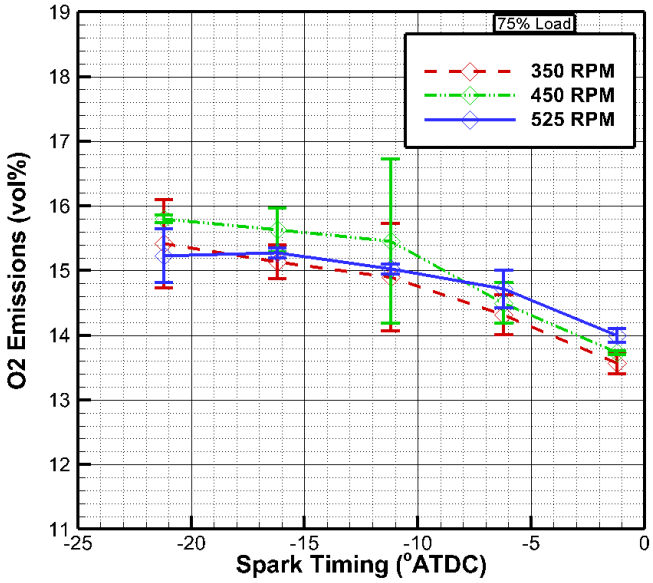

Figure 3-19: O_2 emissions at 75% load

The relationship between speed and oxygen emissions is less apparent, except for the high load, low speed case (Figure 3-18). This outlier is consistent with both the THC and CO_2 emissions results. The inverse relationship shows that the high load, low speed requires the richest equivalence ratio to maintain (Figure 3-19, Figure 3-20). This is qualitatively confirmed by the experiment – this is the hardest configuration to maintain, with the engine on the verge of stalling. Additionally, this is the case with the lone unsustainable data point, further describing the engine's operating behavior.

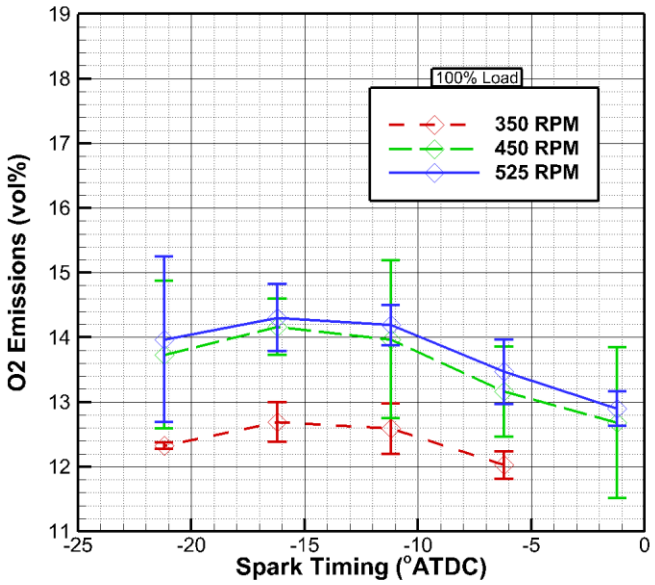

Figure 3-20: O_2 emissions at 100% load

3.1.7 Further Discussion

There is no single engine configuration that reduces all unwanted emissions, as there is a tradeoff between each of their formations. It is helpful to view different test cases against multiple emissions, to directly illustrate this compromise. Natural gas combustion balances a reduction in NOx and THC, with the effects of unburned hydrocarbons especially prevalent in the test engine's two-stroke design. In Figure 3-21: THC vs NOx at 100% load, a unique trend is apparent for both of the higher speed cases. These two conditions at full load are depicted because they are the most common configuration of the Ajax E-565 in the field.

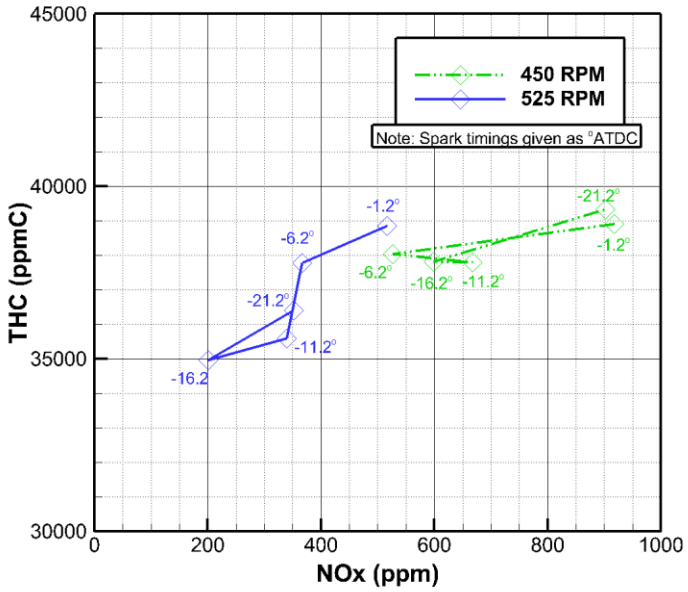

Figure 3-21: THC vs NOx at 100% load

As discussed, NOx formation is temperature driven. There are two mechanisms at play that justify the unique trends seen in the data. First of all, as timing is retarded, the mixture must be richened, bringing the combustion event closer to the peak flame temperature. This is shown clearly from the conventional timing (-11.2 °ATDC) to the fully retarded condition (-1.2 °ATDC), with NOx concentrations increasing. The other side of the curves, from the conventional timing to the fully advanced condition (-21.2 °ATDC), trends with the high peak pressures observed. The net pressure is higher for these cases, as the apex of the combustion pressure curve coincides with the motoring curve of the engine, resulting in higher mixture temperatures.

3.1.8 Pressure Data (Rate of Heat Release)

Pressure data is used in the derivation of the rate of heat release, a value that shows the energy released from the fuel as a function of crank angle. The pressure values used to derive RoHR are found in Appendix D – Pressure Curves. The rate of heat release is derived from Equation 4 and shown for 450 RPM and 525 RPM at 100% load, the most common load case for the Ajax engine in the field.

Figure 3-22: Ajax E-565 timing diagram adds physical relevance to the crank angle position shown in the RoHR curves. Top dead center (TDC) is denoted as 0°, and the condition where the piston is closest to the cylinder head, with a minimum chamber volume. Combustion begins at ignition (varied by spark timing) and carries through the expansion stroke to 120.4°, where the exhaust port lets the burned gas escape the combustion chamber.

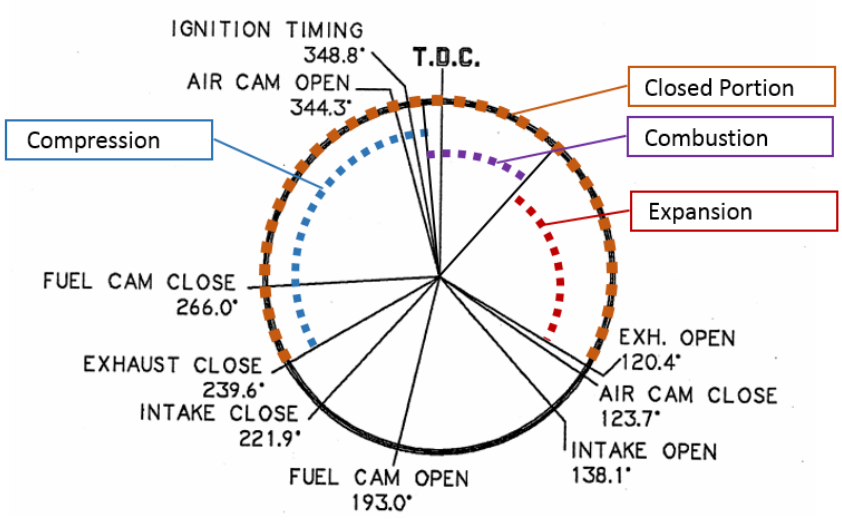

Figure 3-22: Ajax E-565 timing diagram
Courtesy of Thomas Hurley, GE Oil and Gas and Abdullah Bajwa [45]

Roughly 18 CAD later, the intake is opened, allowing a fresh mixture into the chamber and helping to purge burned gases out. This process carries through bottom dead center (BDC) and to the compression stroke, as seen in Figure 3-23 and Figure 3-24.

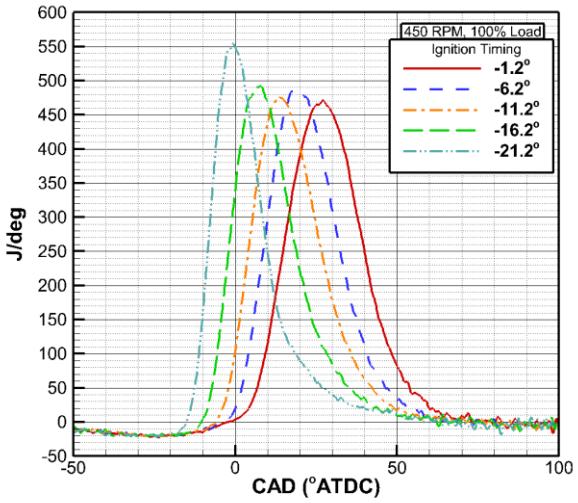

Figure 3-23: Rate of heat released at 450 RPM and 100% load

The RoHR curves start at -50°, during the compression stroke. The initial value is essentially zero for all spark timings. While the mixture is being compressed, it has not released any of its energy yet. The curves begin to rise at the start of combustion, which directly corresponds to spark timing. The curves for both speeds show the fully advanced case reaching its peak heat release very close to TDC, with a large amount of energy released on the expansion stroke. In this case, the combustion process is fighting against the piston, which is detrimental to power output. If timing is advanced too much, it can cause engine knock [46], which can damage internal components. Testing at the

fully advanced configuration showed signs of this, with some firing sequences making this noise.

The two most retarded spark timings have peak energy release too far into the expansion stroke to be able to fully utilize the energy released. This explains why more fuel was needed for these cases to compensate for this lack of efficiency. The emissions that suggest rich mixtures in retarded spark timing cases coincide with this conclusion.

Not surprisingly, the spark timing that the engine is sold with (11.2° BTDC) has a peak heat release rate soon after TDC, near the 20° that is most effective [29]. Based on the rate of heat release data, it would interesting to see a finer resolution between conventional timing and the 5° spark advance case, as this appears to define the useful range of good peak heat release placement.

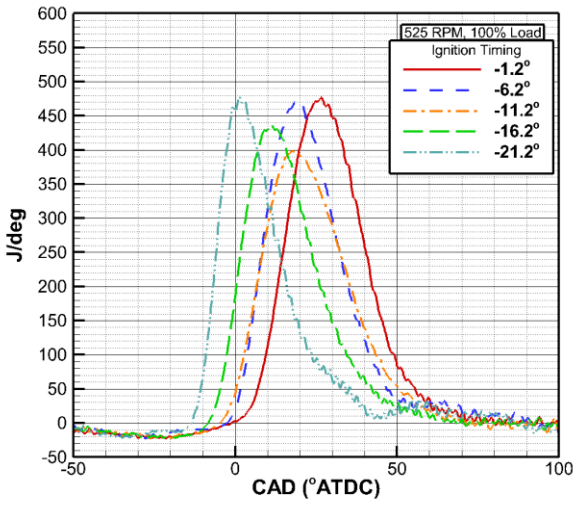

Figure 3-24: Rate of heat released at 525 RPM and 100% load

3.3 Coolant System Study

The coolant flowrate analysis performed by students in the AERL was an industry-first for this engine, and provided useful insight to experts who use this unit regularly. The results for various speeds and loads are found in Table 4: Ajax E-565 coolant flowrates. This study serves to illustrate the parasitic load that the cooling system imposes when not operating in an extreme climate environment, such as the AERL test facility.

Load	Speed	Flowrate (gpm)
Low (150 ft-lb)	Low (375 RPM)	1.43
Low (150 ft-lb)	High (525 RPM)	1.65
High (350 ft-lb)	Low (375 RPM)	1.80
High (350 ft-lb)	High (525 RPM)	2.15

Table 4: Ajax E-565 coolant flowrates

The heat transfer rate as the fluid passes through the radiator illustrates another phenomenon that may explain some trends in the emissions data. NOx values decrease as the engine speed picks up, supporting the observation that the engine has better relative cooling in this case.

Table 5 shows how the high speed, high load case is more effective in cooling, since the fan is spinning faster to remove more heat. This reduces the temperatures in the water jacket around the combustion chamber. Interestingly, the inlet temperature to the radiator (a representation of the heat given off by combustion) is practically the same value for both speeds at while at high load. This suggests that the in-cylinder temperature is higher for the low speed scenario, contributing to an increase in NOx formation.

Load	Speed	Radiator Inlet Temp. [°C]	Radiator Heat Transfer Rate [kW]
Low (150 ft-lb)	Low (375 RPM)	67.8	10.2
Low (150 ft-lb)	High (525 RPM)	68.3	12.7
High (350 ft-lb)	Low (375 RPM)	79.5	14.1
High (350 ft-lb)	High (525 RPM)	80.5	20.6

Table 5: Radiator inlet temperature and heat transfer rate for the load and speed sweep

The fan removes more heat from the engine than necessary during testing in every configuration, as the boiling temperature of the cooling fluid was never realized. This shows the parasitic power loss to the engine to cool itself, at least for the temperate test environment. While the engine is designed for a worst-case scenario, there are many climates that are similar to the AERL. The engine could be modified for milder working conditions to reduce wasted energy.

The emissions study showed strong correlations between NOx and CO_2 production and increased load, both constituents of the exhaust that are harmful. The cooling fan increases the load on the engine, thus possibly contributing to the concentration of these emissions. To confirm this, further work needs to be done to directly reduce parasitic losses to the fan, while also considering the effects of reduced cooling. It is possible that the reduced cooling is more significant in contributing to NOx formation than the reduced engine load would be.

4 CONCLUSIONS

This study considers the implementable changes of modified spark timing and reduced cooling fan loads to an Ajax E-565 natural gas engine. The interest of this study aims to improve the exhaust emissions of natural gas engines already in use, by a seeing the effects of various spark timings and investigating the parasitic losses found in the cooling fan.

The emissions data and rate of heat release curves confirm some expectations had prior to this study. Primarily, there is little to be gained by retarding the start of ignition from where it is originally. This makes the combustion event less effective, occurring farther into the expansion stroke. Also, the additional fuel required to maintain a constant load while the timing is retarded increases fuel consumption. The most advanced timing location of this study, at 21° BTDC, is not a good choice because of the spike in NOx emissions. The heat released from this advanced timing appears premature, occurring too far into the compression stroke.

The two best spark timings of this test are at the original 11.2° BTDC and the 5° advanced 16.2° BTDC. It would be a useful endeavor to repeat this study over a finer range between these two values. Figure 3-21: THC vs NOx at 100% load shows how both emissions are lowest around these spark timings. Also, the heat release rate profile trends with what is known to maximize power for an engine. An advantage to the ignition system on this engine is that a spark timing adjustment is simple and inexpensive – a modified bracket can be installed to shift the spark pickup to adjust

spark timing. This solution aligns with the intent of this study, providing readily implementable change to engines in service.

The cooling system is over-designed for the test environment of this study, wasting energy in turning its own fan. Of course, the test facility does not represent all locations that the engine will be used, but makes a point that for milder environments, a modified cooling system could be specified. The easiest option to implement would be a different sized fan pulley, to adjust how much the fan spins with respect to the engine, and thus reducing parasitic losses. A more complicated, yet precise method would be to actively control the fan on a clutch, to remove the appropriate amount of heat for any situation.

5 FUTURE WORK

The Advanced Engines Research Laboratory at Texas A&M University acquired the Ajax E-565 engine in the summer of 2013. Since becoming operational, this engine has served as a reliable unit to educate both those new to internal combustion engines and experienced enthusiasts alike. The studies done by the group today are paving the foundation for many more investigations by future students. Two modifications are expected to begin at the conclusion of this study: a direct injection retrofit and an increased spark-duration device.

A direct injection system is desired for a variety of reasons. First of all, it is estimated that up to half of the fuel introduced into the cylinder is "short-circuited", or discharged directly to the exhaust. Not only is this a massive waste of fuel, but unburned hydrocarbon emissions are oftentimes worse than their oxidized products of combustion [31]. A DI system also allows for a leaner in-cylinder mixture. This reduces overall fuel consumption, while maintaining sufficient stoichiometric ratios to ensure a stable combustion event [47]. For the purpose of research and development, the DI system allows the user much more controllability of the volume of fuel injected and its timing, making for an interesting study for upcoming students.

Since the Ajax engine is spark-ignited, the other part of the combustion equation is the ignition. Spark energy is often a point of discussion, but studies have found little improvements for these engines by simply increasing the localized spark energy [5]. However, flame propagation improvements have been found in multiple spark plug cylinder heads and prolonged-duration spark events, on the order of 40 CAD [5, 48].

In the future, with regards to the cooling system, a study into various fan pulley sizes could by explored to see how much energy is saved. There is motivation to study this from the results of this investigation. Alternatively, the fan could be retrofit with a controller to more precisely adjust how much heat is being removed.

Finally, there is useful instrumentation that will add accuracy to data collected in future experiments. As much of the temperature-based analysis in this study was done theoretically, an in-cylinder thermocouple would make future experiments more accurate and clarify some of the emissions trends. Also, an electronically controlled gas throttle will enable quantitative assessments as to how much more fuel is needed for the various cases seen in this study.

REFERENCES

1. Brito, A.J. and A.T. de Almeida, *Multi-Attribute Risk Assessment for Risk Ranking of Natural Gas Pipelines.* Reliability Engineering & System Safety, 2009. **94**(2): p. 187-198.

2. Johnson, D., et al. *Evaluation of Spark Plug and Timing Configurations on the Fuel Consumption, Combustion Stability, and Emissions of a Large-Bore, Two-Stroke, Natural Gas Engine*. in *ASME 2016 Internal Combustion Engine Fall Technical Conference*. American Society of Mechanical Engineers.

3. Griffin, A.A., *Combustion Characteristics of a Two-Stroke Large Bore Natural Gas Spark-Ignited Engine*. 2015, Texas A&M University: Master of Science Thesis.

4. *Natural Gas: A Summary of the History, Uses, and Consumption with a Discussion on the Influence of Domestic Shale Drilling.* 2011: National Energy Technology Labs.

5. Wood, C.D. and J.K. Kubesh, *Evaluation of Emissions Control Technology for Reciprocating Integral Engine-Compressor Units.* SwRI Report for Tenneco Gas Environmental and Technology Department, 1995.

6. Cameron, *Desciption of Ajax Engines*. 2012: AJAX Products Group.

7. Blair, G.P., *Design and Simulation of Two-Stroke Engines*. 1996: Society of Automotive Engineers Warrendale, PA.

8. Cameron, *Ajax® E-565 Gas Engine Service Manual*. 2012.

9. Arcoumanis, C. and C.S. Bae, *Correlation Between Spark Ignition Characteristics and Flame Development in a Constant-Volume Combustion Chamber*. 1992, SAE Technical Paper.

10. Kubesh, J.T., D.J. Podnar, and C.P. Colucci, *Lean Limit and Performance Improvements for a Heavy-Duty Natural Gas Engine*. 1996, SAE Technical Paper.

11. McAllister, C.D. and T.W. Simpson, *Multidisciplinary Robust Design Optimization of an Internal Combustion Engine.* Journal of mechanical design, 2003. **125**(1): p. 124-130.

12. Mashayekh, A., et al., *Prediction of Air–Fuel Ratio Control of a Large-Bore Natural Gas Engine Using Computational Fluid Dynamic Modeling of Reed Valve Dynamics.* International Journal of Engine Research, 2017.

13. Harrington, J.A. and R.C. Shishu, *A Single-Cylinder Engine Study of the Effects of Fuel Type, Fuel Stoichiometry, and Hydrogen-to-Carbon Ratio on CO, NO, and HC Exhaust Emissions*. 1973, SAE Technical Paper.

14. Ernst, A. and J.D. Zibrak, *Carbon Monoxide Poisoning.* New England Journal of Medicine, 1998. **339**(22): p. 1603-1608.

15. Newhall, H.K. *Kinetics of Engine-Generated Nitrogen Oxides and Carbon Monoxide*. in *Symposium (International) on Combustion*. 1969. Elsevier.

16. Horiba, *CO/CO2 (HC,NO,N2O,CO2) Analyzer; AIA-72X Series*. 2007.

17. NVGAmerica. *Environmental Benefits*. 2014; www.ngvamerica.org.

18. Brandt, A.R., et al., *Methane Leaks from North American Natural Gas Systems.* Science, 2014. **343**(6172): p. 733-735.

19. Hannon, D., *Compressor Cylinder Emissions Reduction*, in *Gas Machinery Conference* A. Corporation, Editor. 2015: Austin, TX.

20. Nuti, M. and L. Martorano, *Short-Circuit Ratio Evaluation in the Scavenging of Two-Stroke SI Engines*. 1985, SAE Technical Paper.

21. Horiba, *THC Analyzer; FIA-725A*. 2003.

22. Horiba, *Instruction Manual for CLA-220 Chemiluminescent Analyzer*. 1995. p. 2.

23. Haagen-Smit, A.J. and M.M. Fox, *Automobile Exhaust and Ozone Formation*. 1955, SAE Technical Paper.

24. Miller, R., et al., *A Super-Extended Zel'dovich Mechanism for NOx Modeling and Engine Calibration*. 1998, SAE Technical Paper.

25. Turns, S.R., *An Introduction to Combustion*. Vol. 287. 1996: McGraw-Hill New York. p. 569.

26. Horiba, *NO/NOx Analyzer; CLA-720MA*. 2003.

27. De Klein, C.A.M., C. Pinares-Patino, and G.C. Waghorn, *Greenhouse Gas Emissions.* Environmental Impacts of Pasture-Based Farming, 2008: p. 1-33.

28. Horiba, *O2 Analyzer; MPA-720*. 2002.

29. Heywood, J., *Internal Combustion Engine Fundamentals*. 1988: McGraw-Hill Education.

30. Heywood, J., *Pollutant Formation and Control.* PECS, 1976.

31. Parker, T. *Fugitive Methane Emission Reduction Using Gas Turbines*. American Society of Mechanical Engineers.

32. Varde, K.S., et al., *Emissions and Their Control in Natural Gas Fueled Engines*. 1992, SAE Technical Paper.

33. Gatowski, J.A., et al., *Heat Release Analysis of Engine Pressure Data*. 1984, SAE Technical Paper.

34. Beshouri, G.M., *Combustion Pressure Based Emissions Monitoring and Control for Large Bore IC Engines: An Alternative Parametric Emissions Models (PEMS) Methodology.* ASME Paper, 1998.

35. Brown, J., T. Kroeger, and S. Chakravarthy, *Instrumenting a Thermosiphon Cooling System on a Large-Bore Two-Stroke Spark Ignited Natural Gas Engine* 2016.

36. Temprel, *How to Choose a Thermocouple*, O.R.P.C. Type, Editor. 2016: www.temprel.com.

37. Ceviz, M.A. and M. Akın, *Design of a New SI Engine Intake Manifold with Variable Length Plenum.* Energy Conversion and Management, 2010. **51**(11): p. 2239-2244.

38. Taylor, *DEA150 Air Cooled Eddy Current Dynamometer*, in *Operation & Maintenance Manual*. 2015.

39. Matekunas, F.A., *Modes and Measures of Cyclic Combustion Variability*. 1983, SAE Technical Paper.

40. Heywood, J.B. and E. Sher, *The Two-Stroke Cycle Engine.* Warrendale, PA: Society of Automotive Engineers, 1999: p. 472.

41. Griffin, A.A., et al., *Impact of Cyclic Variation on Emissions in a Two-Stroke Large Bore Natural Gas Spark-Ignited Engine*, in *Gas Machinery Conference*. 2016: Denver, CO. p. 23.

42. Hoekstra, R.L., P. Van Blarigan, and N. Mulligan, *NOx Emissions and Efficiency of Hydrogen, Natural Gas, and Hydrogen/Natural Gas Blended Fuels*. 1996, SAE Technical Paper.

43. Tompkins, B.T., *Emissions Comparison Between Petroleum Diesel and Biodiesel in a Medium-Duty Diesel Engine*. 2008, Texas A&M University: Master of Science Thesis.

44. Riegel, J., H. Neumann, and H.M. Wiedenmann, *Exhaust Gas Sensors for Automotive Emission Control.* Solid State Ionics, 2002. **152**: p. 783-800.

45. Bajwa, A.U., *First and Second Law Analyses of a Large Bore Two Stroke Spark Ignition Engine Fueled with Natural Gas*, in *Mechanical Engineering*. 2016, Texas A&M University: Master of Science Thesis.

46. Brunt, M.F.J., C.R. Pond, and J. Biundo, *Gasoline Engine Knock Analysis Using Cylinder Pressure Data*. 1998, SAE Technical Paper.

47. Zeng, K., et al., *Combustion Characteristics of a Direct-Injection Natural Gas Engine Under Various Fuel Injection Timings.* Applied Thermal Engineering, 2006. **26**(8): p. 806-813.

48. King, S.R. and W.E. Liss, *Effects of Spark Plug Number and Location in Natural Gas Engines.* Journal of Engineering for Gas Turbines and Power, 1992. **114**: p. 475.

49. Beckwith, T.G., R.D. Marangoni, and J.H. Lienhard, *Mechanical Measurements*. Vol. 768. 2007: Pearson Prentice Hall Upper Saddle River, NJ.

50. Fox, R.W., Alan T. McDonald, and Philip J. Pritchard, *Fluid Mechanics*. Vol. Eighth. 2012: Wiley and Sons Ltd

51. Cengel, Y.A. and M.A. Boles, *Thermodynamics: An Engineering Approach.* Sea, 2002. **1000**: p. 8862.

APPENDIX A - GAS COMPOSITION REPORT

Raw Results Meter: 04016300 04016300S1 Date: 02/01/2017 07:25:40

	Component	Response Factor	UnNorm %	Norm %	Peak Areas	Peak Heights	Peak Times	Liquids (USgal/MCF)	Ideal (Btu/SCF)	Relative Density
1	Propane	2.267	0.241	0.240	980997	10936	49.775	0.066	6.041	0.004
2	Hydrogen Sulfide	0	0	0	0	0	0.000	0	0	0
3	IsoButane	1.844	0.016	0.016	75741	681	71.500	0.005	0.533	0
4	Butane	7.994	0.026	0.026	124073	1018	80.100	0.008	0.860	0.001
5	NeoPentane	0	0	0	0	0	0.000	0	0	0
6	IsoPentane	0.307	0.009	0.009	47076	240	138.075	0.003	0.349	0
7	Pentane	1.419	0.008	0.008	44429	186	160.450	0.003	0.314	0
8	Hexane+	0.179	0.019	0	125750	1435	21.300	0	0	0
9	Nitrogen	3.857	1.687	1.679	4750490	57520	41.250	0	0	0.016
10	Methane	1.116	93.903	93.481	200542712	749915	51.225	0	944.153	0.518
11	CarbonDioxide	1.102	0.992	0.987	3317727	14287	94.025	0	0	0.015
12	Ethane	0.883	3.551	3.535	13511560	27034	217.725	0.942	62.562	0.037
13	Hexane	0	0	0.009	0	0	0.000	0.004	0.439	0
14	Heptane+	0	0	0	0	0	0.000	0	0	0
15	Heptane	0	0	0.009	0	0	0.000	0.004	0.508	0
16	Octane	0	0	0	0	0	0.000	0	0	0
17	Nonane+	0	0	0	0	0	0.000	0	0	0
18	Nonane	0	0	0	0	0	0.000	0	0	0
19	Decane	0	0	0	0	0	0.000	0	0	0
20	Undecane	0	0	0	0	0	0.000	0	0	0
21	Dodecane	0	0	0	0	0	0.000	0	0	0
22	Ethane-	0	0	0	158018313	1552294	32.350	0	0	0
23	Propane +	0	0	0	1338666	13697	28.500	0	0	0
24	Oxygen	0	0	0	0	0	0.000	0	0	0
25	Total		100.452	100.000				1.036	1015.760	0.591

Compressibility:	0.998
Density:	0.045 (lbm/ft3)
Real RD:	0.592
Ideal CV:	1015.760 (Btu/SCF)
Inferior Wobbe:	1294.894 (Btu/SCF)
Superior Wobbe:	1318.535 (Btu/SCF)
Inferior CV:	997.017 (Btu/SCF)
Superior CV:	1014.737 (Btu/SCF)

APPENDIX B - INSTRUMENTATION

Dynamometer Load Cell Calibration

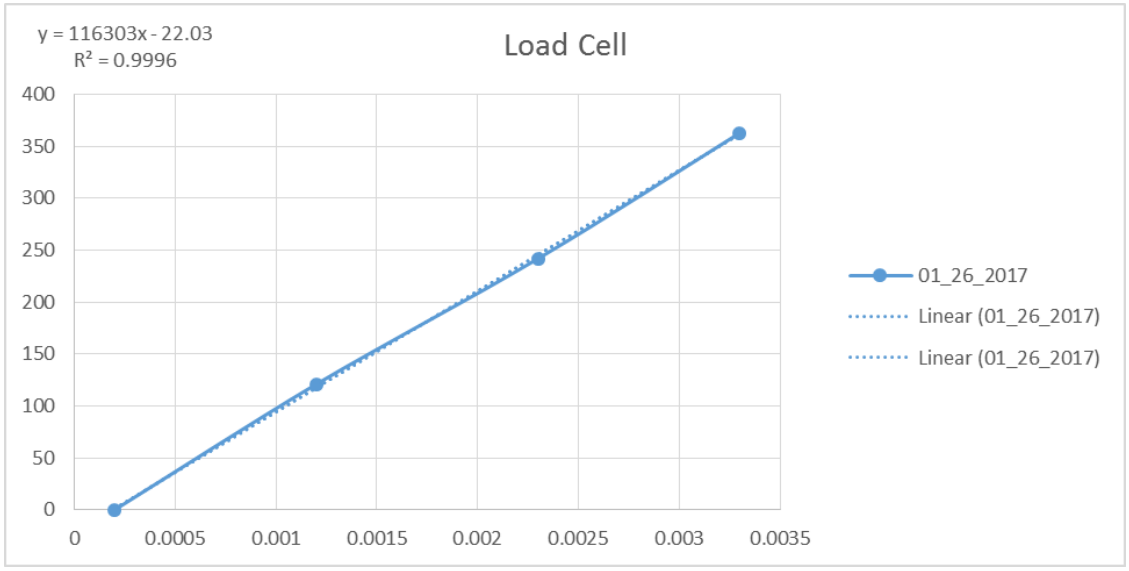

Figure B-1: Dynamometer load cell linearity

MEXA-7100D Error

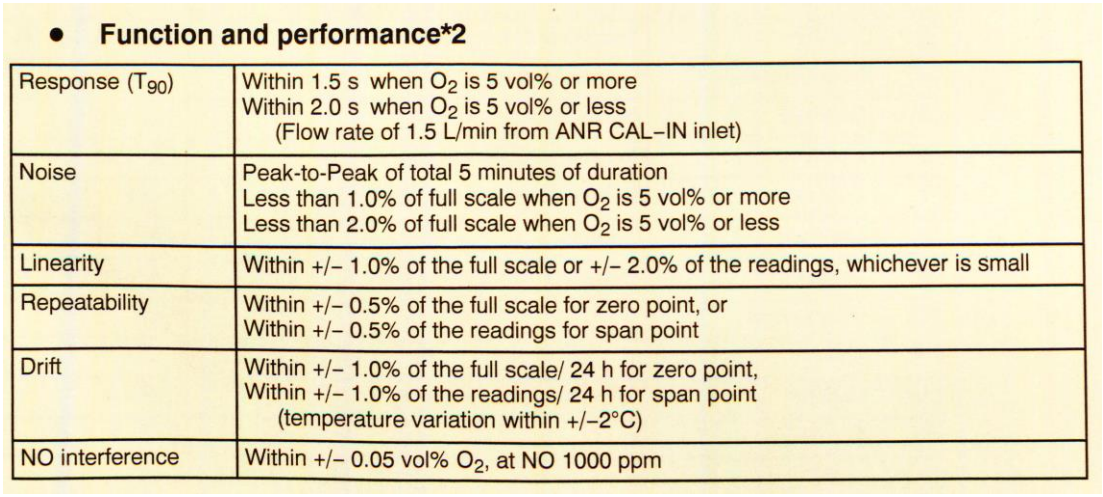

- **Function and performance*2**

Response (T_{90})	Within 1.5 s when O_2 is 5 vol% or more Within 2.0 s when O_2 is 5 vol% or less (Flow rate of 1.5 L/min from ANR CAL–IN inlet)
Noise	Peak-to-Peak of total 5 minutes of duration Less than 1.0% of full scale when O_2 is 5 vol% or more Less than 2.0% of full scale when O_2 is 5 vol% or less
Linearity	Within +/– 1.0% of the full scale or +/– 2.0% of the readings, whichever is small
Repeatability	Within +/– 0.5% of the full scale for zero point, or Within +/– 0.5% of the readings for span point
Drift	Within +/– 1.0% of the full scale/ 24 h for zero point, Within +/– 1.0% of the readings/ 24 h for span point (temperature variation within +/–2°C)
NO interference	Within +/– 0.05 vol% O_2, at NO 1000 ppm

Figure B-2: Oxygen analyzer error

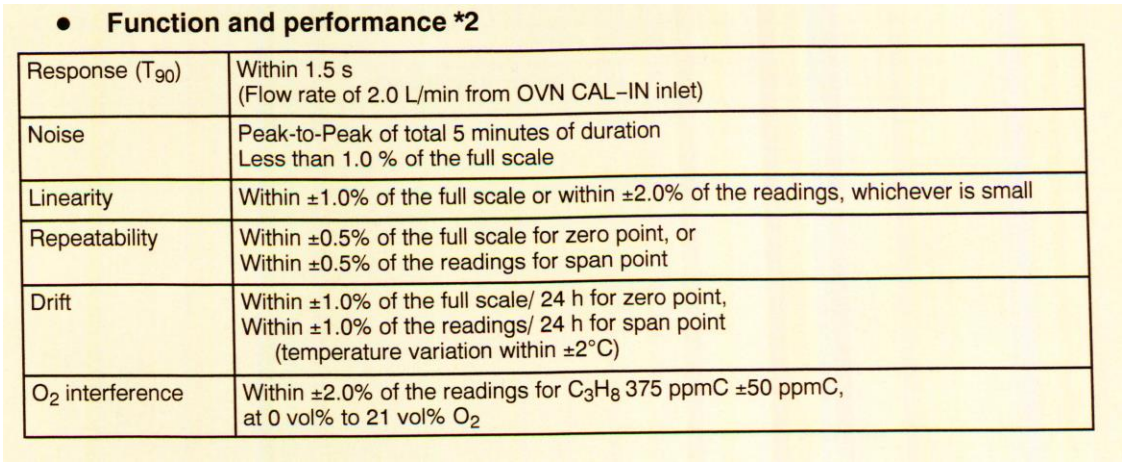

- **Function and performance *2**

Response (T_{90})	Within 1.5 s (Flow rate of 2.0 L/min from OVN CAL–IN inlet)
Noise	Peak-to-Peak of total 5 minutes of duration Less than 1.0 % of the full scale
Linearity	Within ±1.0% of the full scale or within ±2.0% of the readings, whichever is small
Repeatability	Within ±0.5% of the full scale for zero point, or Within ±0.5% of the readings for span point
Drift	Within ±1.0% of the full scale/ 24 h for zero point, Within ±1.0% of the readings/ 24 h for span point (temperature variation within ±2°C)
O_2 interference	Within ±2.0% of the readings for C_3H_8 375 ppmC ±50 ppmC, at 0 vol% to 21 vol% O_2

Figure B-3: Total hydrocarbon analyzer error

● **Function and performance*2**

Response (T_{90})	AIA-721 series: Within 2.0 s (at the flow rate of 3 L/min from ANR CAL-IN inlet) AIA-722, 723 series: Within 1.5 s (at the flow rate of 2 L/min from ANR CAL-IN inlet)
Noise	Peak-to-Peak of total 5 minutes of duration less than 1.0% of the full scale
Linearity	Within ±1.0% of the full scale or ±2.0% of the readings, whichever is small
Repeatability	Within ±0.5% of the full scale for zero point, or within ±0.5% of the readings for span point
Drift	Within ±1.0% of the full scale/24 h for zero point, Within ±1.0% of the readings/24 h for span point (temperature variation within ±2°C)

Figure B-4: Carbon monoxide/carbon dioxide analyzer error

● **Function and performance*3**

Response (T_{90})	NO line: Within 2.0 s (50 ppm or more), within 2.5 s (less than 50 ppm) NOx line: Within 2.5 s (50 ppm or more), within 3.0 s (less than 50 ppm) (Supplying flow rate of 2 L/min from OVN CAL inlet)
Noise	Peak-to-Peak of total 5 minutes of duration Less than 2.0% of the full scale (excluding spike noise of once/ hour)
Linearity	Within +/−1.0% of the full scale or +/− 2.0% of the readings, whichever is small
Repeatability	Within +/−0.5% of the full scale for zero point, or Within +/−0.5% of the readings for span point
Drift	Within +/−1.0% of the full scale / 24 h for zero point, Within +/−1.0% of the readings / 24 h for span point (temperature variation within +/−2°C)
CO_2 Interference	Within −0.19% of the readings, at 1 vol% interfering CO_2
H_2O Interference	Within −2.0% of the readings, at 25°C H_2O saturation

Figure B-5: Nitrogen oxides analyzer error

APPENDIX C - CALCULATIONS

Error in Emissions Measurements

Uncertainty in emissions data is given as a 95% confidence interval based on the mean and standard deviation of each test condition. Each condition was observed twice (N=2).

From Student's t-Table (for a 95% confidence interval) [49]:

$$z\alpha_{/2} = 1.96$$

$$\bar{x} \pm z\alpha_{/2} \frac{S}{\sqrt{N}}$$

This error margin defines the error bars above and below the mean for each data point.

Coolant Flowrate

The mass flow rate of the coolant is derived from the continuity equation, Bernoulli's equation, and venturi flowmeter specifications [50]:

$$\dot{m} = \rho v A$$

$$\dot{m} = \rho \frac{\pi}{4} D_{throat}^2 \frac{C}{\sqrt{1-\beta^4}} Y \sqrt{\frac{2\Delta P}{\rho}}$$

Heat Transfer Rate

The coolant flowrate previously derived is used in the heat transfer rate equation [51]:

$$\dot{Q} = \dot{m} c_p \Delta T$$

APPENDIX D - PRESSURE CURVES

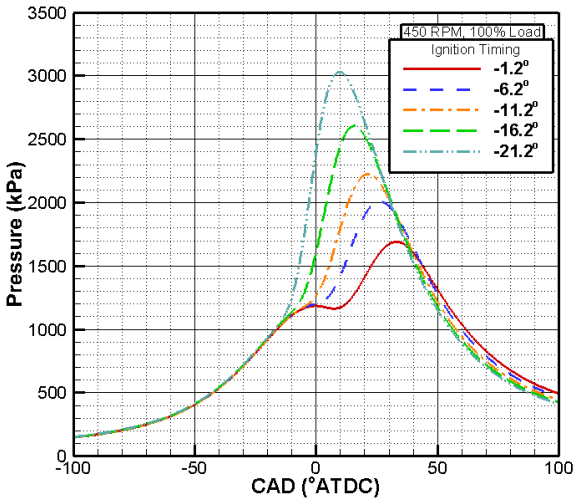

Figure D-1: Pressure curves from 450 RPM and 100% load

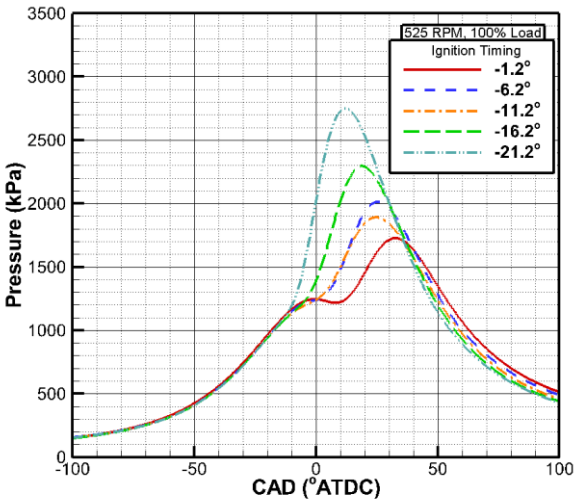

Figure D-2: Pressure curves from 525 RPM and 100% load

APPENDIX E - VITA

Jeffrey Brown graduated cum laude from Texas A&M University in May of 2015 with a Bachelor of Science in Mechanical Engineering before beginning his graduate studies at Texas A&M in the Advanced Engines Research Lab. He will graduate in May of 2017 with a Master of Science in Mechanical Engineering and then begin working with General Motors in Detroit, Michigan.